Materials Advances

ROYAL SOCIETY OF CHEMISTRY

REVIEW

View Article Online
View Journal | View Issue



Cite this: *Mater. Adv.*, 2023, 4, 4294

# Incorporation of functional polymers into metal halide perovskite thin-films: from interactions in solution to crystallization

Antonella Giuri, *[ab] Nadir Vanni,[a] Muneeza Ahmad, [c] Nicholas Rolston, [c] Carola Esposito Corcione,[b] Andrea Listorti, [d] Silvia Colella[e] and Aurora Rizzo *[a]

In the last decade, metal halide perovskite materials (MHPs) have presented several innovative opportunities for optoelectronic technologies, particularly for solar cells. However, challenges related to reliable material processability, combined with inherent instability, pose major roadblocks in the path towards the industrialization of MHP-based technologies. One of the strategies, developed to overcome these issues, is the incorporation of polymeric additives to control the crystallization process of the material, which represents a key aspect for reproducible manufacturing of robust films. Owing to the vast range of properties presented by polymeric materials, a judicious selection of polymers and perovskite compositions allows tailoring the physical–chemical–mechanical properties of the final composite to the desired device application. In this review, the recent advances on polymer inclusion into perovskite photoactive layers for solar cells are discussed. Following a brief introduction to perovskite fundamental properties for photovoltaic applications, the focus is on the self-assembly process of MHPs and on the use of polymers with different functionalities as templating agents for the growth of polycrystalline films with optimal optoelectronic quality. The influence of different polymers on the stability, mechanical behavior and processability of MHPs is then rationalized. Finally, a summary of the most significant and accessible characterization techniques used to investigate the polymer–perovskite-based composite is given, providing guidelines for the further development of innovative formulations.

Received 4th August 2023,
Accepted 5th September 2023

DOI: 10.1039/d3ma00506b

rsc.li/materials-advances



## 1. Introduction

The use of metal halide perovskite semiconductors has led to impressive progress in the field of optoelectronics, in particular photovoltaics, where MHP-based devices reached an impressive certified power conversion efficiency (PCE) of 25.8%.[1–4] This progress is due to the incredible properties of these materials, such as high absorption coefficient, low exciton binding energy, high charge carrier mobility, and long carrier diffusion length.[5–9] Additionally, these properties can be easily tuned by modifying the material composition, specifically targeting several applications, from solar cells,[10,11] light-emitting diodes,[12,13] photodetectors,[14] to X-ray detectors.[15,16] Another peculiar characteristic of MHPs is their low temperature and simple solution-processability with scalable fabrication techniques, spanning from ink jet printing,[17,18] to spray coating,[19,20] to slot-die, gravure printing, screen printing, etc.[21–25] However, the commercialization of perovskite-based technologies is still hindered by major challenges mainly related to the accurate and reliable control of material crystallization as well as environmental and thermomechanical stability.

Over the past few years, many polymers were tested as additives in perovskite-based optoelectronic devices, exploiting their interaction with the MHP precursors and their intrinsic mechanical robustness, aiming at improving the formation and stability of MHPs toward manufacturing.[26–36]

In general, perovskite self-assembly starts from a solution containing the material precursors. For the benchmark perovskite material methylammonium lead iodide ($MAPbI_3$), the precursors are $PbI_2$ and MAI. Herein, the formation of high-order iodoplumbate coordination complexes ($PbI^{3-}$, $PbI_4^{2-}$, *etc.*), following the complexation of $PbI_2$ by iodine, act as initial seeds during $PbI_6^{4-}$ octahedra formation, eventually influencing the crystallinity, morphology and defect density of the

[a] *CNR NANOTEC – Istituto di Nanotecnologia, c/o Campus Ecotekne, Via Monteroni, 73100 Lecce, Italy. E-mail: antonella.giuri@nanotec.cnr.it, aurora.rizzo@nanotec.cnr.it*
[b] *Dipartimento di Ingegneria dell'Innovazione, Università del Salento, via per Monteroni, km 1, 73100, Lecce, Italy*
[c] *Arizona State University – Ira A. Fulton Schools of Engineering, Tempe, AZ, 85284, USA*
[d] *Dipartimento di Chimica, Università di Bari, Via Orabona 4, 70126 Bari, Italy*
[e] *CNR NANOTEC – c/o Dipartimento di Chimica, Università di Bari, Via Orabona 4, 70126 Bari, Italy*

resulting perovskite films.[37–40] The role of the polymer in this complex system is mainly to control and guide perovskite growth through precursor interactions.[26,27,29,32–35,41] Afterwards, in the film, polymers can act as mechanical reinforcement,[31] and improve thermal stability[32] or moisture stability with self-healing properties.[34] Therefore, a judicious selection of the polymer is fundamental to achieve the desired goal and to determine the efficacy of the developed approach.

In this review, recent progress in the design and use of polymers for perovskite-based solar cells is discussed. The influence of polymer inclusion in perovskite formulations is evaluated, mainly focusing on the control of the crystallization process, then on the beneficial effects induced on perovskite properties, including device performance, stability and processability. Finally, a summary of the main characterization tools used to investigate perovskite crystallization is provided, from the preliminary interactions occurring in solution to the perovskite film formation.

## 2. Metal halide perovskites: an overview

### 2.1. Material structure and properties

The name 'Perovskite' refers to materials whose crystal structure is the same as that of $CaTiO_3$, identified with the general molecular formula $ABX_3$,[42] characterized by a network of corner-sharing $BX_6$ octahedra surrounding a larger A-site cation as shown in Fig. 1(a).[43] Within this class of materials, MHPs consist of A-site organic cations (*i.e.* $CH_3NH_3^+$, $CH(NH_2)_2^+$, $CH_3CH_2NH_3^+$) or inorganic alkyl metal cations (*i.e.* $Cs^+$, $Rb^+$) placed in the body-centered, B-site metal cation (*i.e.* $Pb^{2+}$, $Sn^{2+}$, $Ge^{2+}$) at the corners and X-site anions (*i.e.* $F^-$, $Cl^-$, $Br^-$, $I^-$) at the face-center positions.

In the 1920s, Goldsmith described for the first time the perovskite structure,[44] defining a geometric parameter, the tolerance factor $t$, as follows:

$$t = \frac{r_A + r_X}{\sqrt{2}(r_B + r_X)} \quad (1)$$

where $r_A$, $r_B$ and $r_X$ are the ionic radius for A, B and X ions, as shown in Fig. 1(a).

When $t$ = 1, the perovskite has an ideal cubic structure; meanwhile, when the A-ion is small or the B-ion is large, the tolerance factor ($t$) decreases below 1, and orthorhombic, rhombohedral, or tetragonal structures are formed[43] (Fig. 1(b)). The use of large A-ions induces the formation of layered 2D or 1D perovskites. Mixing A-ions leads to the formation of interesting superstructures, compositions, and stoichiometries, *e.g.* Ruddlesden–Popper, Aurivillius, and Dion–Jacobson phases.[45]

The first composition explored for photovoltaics was Methylammonium lead iodide perovskite ($MAPbI_3$) with a band gap of ~1.6 eV, close to the optimal value for single-junction solar cells, high optical absorption coefficient and good electrical transport properties.[47] The tunability of the composition allows the optoelectronic and physical properties of the materials to be engineered, as shown for the bandgap in Fig. 2, making them suitable for different applications. By replacing the MA cation with the slightly larger formamidinium ion ($CH(NH_2)_2^+$, FA) the band gap decreases down to ~1.4–1.5 eV,[48] making formamidinium lead iodide ($FAPbI_3$) perovskite the ideal active material for single junction solar cell devices.[48] Meanwhile, the replacement of iodine with halides with smaller ionic radii such as chlorine and bromine increases the band gap values up to ~2.3 eV for the $MAPbBr_3$ perovskite and ~3.1 eV for the $MAPbCl_3$ perovskite, making them suitable for tandem solar cell applications and light emitting devices, respectively.

### 2.2. Crystallization process

In general, metal halide perovskite precursor solutions are defined as colloidal dispersions made of a soft coordination complex between inorganic/organic ionic species.[40,51] The most

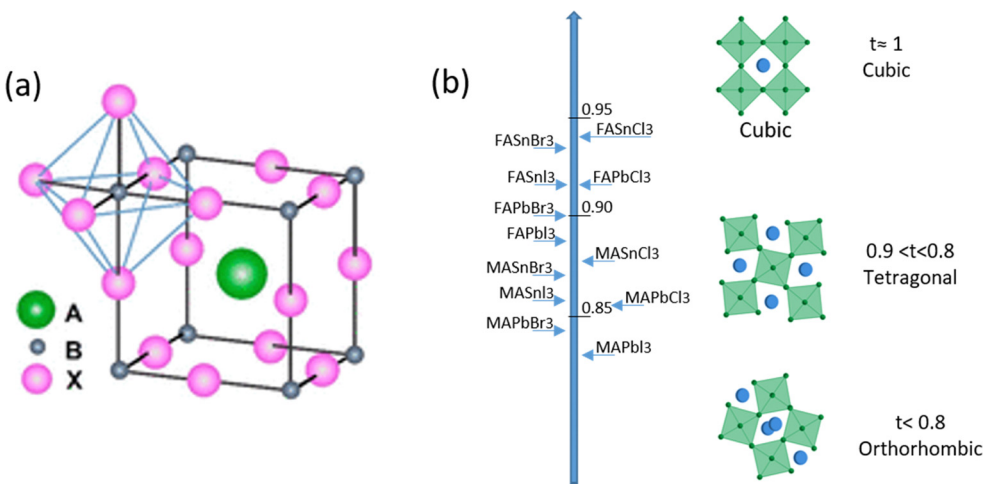


Fig. 1 (a) A sketch of the typical $ABX_3$ perovskite structure. (b) Tolerance factor along with perovskite distortion as a function of composition, from orthorhombic to cubic. Reproduced from ref. 46 with permission from Elsevier, copyright 2014 under a Creative Commons Attribution 4.0 International License (CC BY 4.0).

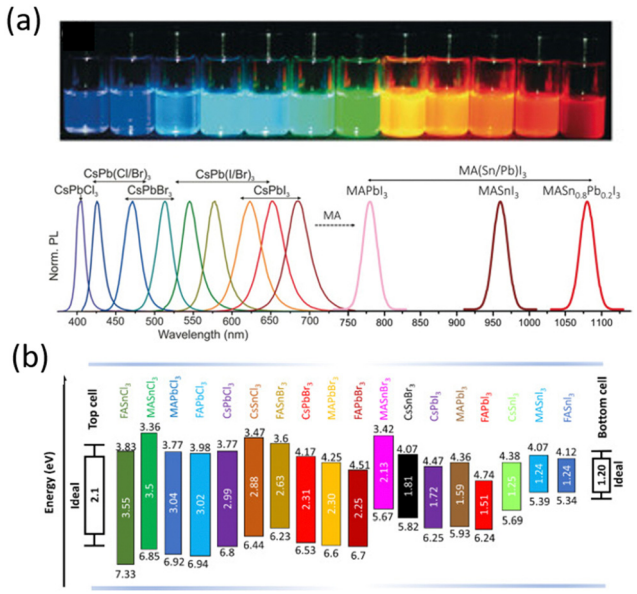


Fig. 2 (a) Photoluminescence tunability of metal halide perovskites. Photographs taken on the precursor solution with different perovskite compositions. Reproduced from ref. 49 with permission from Wiley, copyright 2018 (b) schematic energy level diagram of different metal halide perovskites along with ideal bandgap values. Reproduced from ref. 50 with permission from Elsevier, copyright 2021.

commonly used solvents for solubilizing perovskite precursors are polar solvents with high boiling points (*e.g.*, dimethylformamide (DMF), DMSO, *N*-methyl-2-pyrrolidone (NMP) *etc.*) and slow evaporation rates.

After deposition on a substrate, evaporation of the solvents leads to supersaturation of the precursor concentration, inducing the crystallization process of the halide perovskite in two steps, nucleation from self-seeding and crystal growth. Therefore, good control of the formation process is crucial for obtaining films with suitable morphology, crystallinity, and low defect density for high-performance devices.

From a theoretical point of view, different theories are correlated with the crystallization of solution-processed perovskite thin films, as detailed in the following sections.

**2.2.1. Classical nucleation theory.** Following the classical nucleation theory for homogeneous nucleation, the nuclei are effectively treated as a perfect sphere for which the total free energy is defined as follows:

$$\Delta G = \Delta G_S + \Delta G_V = 4\pi r^2\gamma + \frac{4}{3}\pi r^3 \Delta G_V \qquad (2)$$

where $\Delta G$ is the difference between the free energy of the surface and the volume of the nuclei, and $\Delta G_V$ is the free energy per unit volume, that is the difference between the free energy of monomers in the nuclei and monomers in solution;[52,53] $r$ is the radius of the sphere and $\gamma$ is the surface free energy per unit area. When the nuclei reach the critical radius $r^*$, they are thermodynamically stable and can act as seeds for growth, whereas if the radius of the monomer aggregates is smaller than $r^*$ they dissolve again, decreasing the free energy (Fig. 3a). The nucleation rate increases

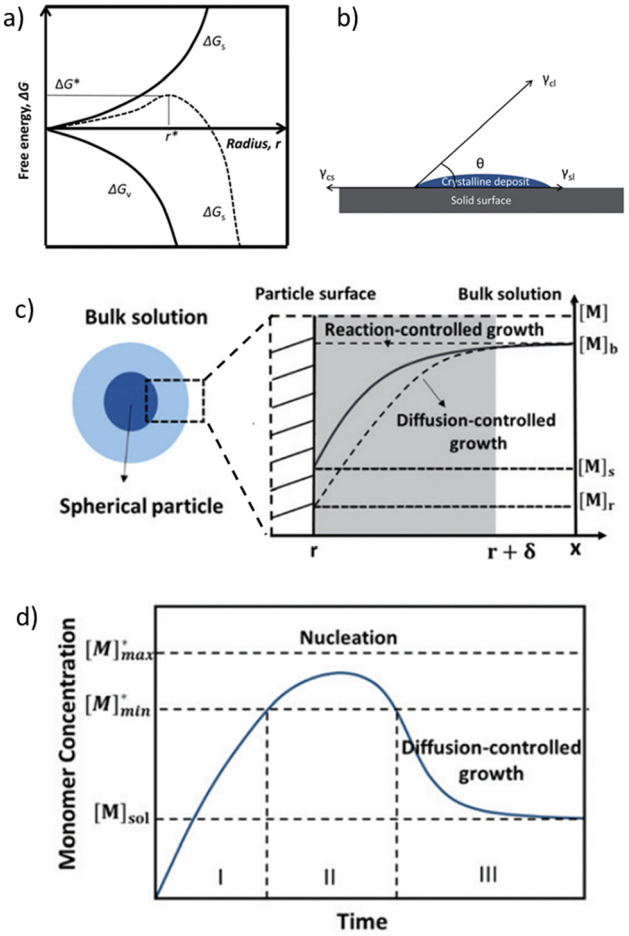


Fig. 3 (a) Diagram of classical nucleation theory. The free energy, $\Delta G$, as a function of the nuclear radius, $r$, for homogeneous nucleation is reported. The critical radius, $r^*$, is also indicated. (b) A sketch of the contact angle, $\theta$, for heterogeneous nucleation onto a substrate. Reproduced from ref. 52 with permission from the Royal Society of Chemistry (c) a scheme of the diffusion layer near the surface of a particle and the monomer concentration as a function of the distance, $x$. (d) LaMer diagram explaining nucleation and growth in the time course. Reproduced from ref. 53 with permission from the Royal Society of Chemistry.

when the degree of supersaturation level and the temperature are increased or if the surface energy is decreased. In a real system, the presence of impurities or bubbles, defined as active centers, may act as heterogeneous nucleation sites, lowering the nucleation energy barrier and speeding up the nucleation process.

In the specific case of perovskite thin films, for which crystallization occurs directly onto a substrate, the interfacial energy diagram consists of three phases: (i) the interfacial energy between the liquid phase and the crystalline phase ($\gamma_{cl}$); (ii) the interfacial energy between the substrate surface and the crystalline phase ($\gamma_{cs}$); and (iii) the interfacial energy between the substrate surface and the liquid phase ($\gamma_{sl}$) (Fig. 3b). If the contact angle ($\theta$) of the solution on the substrate is less than 180°, the nuclei and the active centers have a high affinity, decreasing the interface energy and consequently the nucleation energy barrier. Thus, the free energy of the heterogeneous

nucleation process can be defined as follows:

$$\Delta G^*_{\text{hetero}} = \Phi \Delta G^*_{\text{homo}} = \frac{(2+\cos\theta)(1-\cos\theta)^2}{4}\Delta G^*_{\text{homo}} \quad (3)$$

where $\Phi$ is related to the contact angle $\theta$, suggesting that the affinity between the solution and the substrate has a role in the nucleation process as well.

Following the nucleation step, the crystal growth starts from the formed nuclei and eventually a complete conversion to crystalline perovskite occurs during thermal annealing.

The growth of the particles is a two-step process that involves the transport of monomers from the bulk solution to the crystal surface and the reaction of the monomers on the particle surface.[53] For the growth of crystals in solution, monomer diffusion can be derived from Fick's first law, as follows:[54]

$$J = 4\pi Dr([M_b] - [M_s]) \quad (4)$$

where $J$ stands for the total flux of growing monomers, $D$ is the diffusion coefficient, $r$ represents the radius of the sphere and $[M]_b$ and $[M]_s$ are the respective bulk and the surface concentration of the monomers in the solution. A similar expression can be derived for the surface reaction rate, $k$, which is assumed to be independent of the radius of the particles.

$$J = 4\pi r^2 k([M_s] - [M_r]) \quad (5)$$

where $[M]_r$ is the solubility of the particle with a radius $r$ (particles with a larger radius are less soluble). Given eqn (4) and (5), the crystal growth process can be limited either by the diffusion of monomers or by the surface reaction rate. Diffusion-controlled growth speeds up the formation of particles with uniform dimensions. In surface-controlled growth, the surface reaction rate is very slow and the concentration of monomers on the surface is close to the monomer concentration in the bulk (see Fig. 3c).

**2.2.2. La Mer model.** One of the most used theories to model the nucleation and growth of MHP material from solution is the La Mer model. The La Mer diagram, shown in Fig. 3d, represents the time evolution of the monomer concentration at a constant evaporation rate of the solvent and temperature. The diagram can be divided into three parts: (I) the concentration of the monomers increases in the solution; (II) supersaturation occurs when the monomer concentration overcomes the critical value ([$M$]*min); (III) the growth process starts as nuclei form, and the growth rate is controlled by the diffusion of growing species. The nucleation and the growth processes end when the monomer concentration decreases below the critical value and the solubility value ([$M$]sol), respectively.[53]

**2.2.3. Ostwald ripening model.** Another general model used to explain perovskite formation is Ostwald ripening.[55] Given the Gibbs–Thomson relationship that correlates the solubility of the growth species with their size: the smaller particles have higher surface energy and solubility, whereas the larger particles are less soluble.[54] The growth process in this case occurs by redissolution of the smaller growing particles and re-deposition of the dissolved monomers on the surface of the larger growing ones. This makes the larger particles to grow further. In MHP materials, the residual solvent participating in the formation of the intermediate phase (*e.g.* MAI-dimethyl sulfoxide (DMSO)-$PbI_2$) can be released. This promotes film formation by dissolving the perovskite seeds with smaller sizes, which then grow on the larger seeds and result in adjacent grain coarsening.[56–58]

A good balance between the nucleation and growth processes is achievable by controlling the drying kinetics of the perovskite precursor solution, inducing a higher degree of supersaturation, speeding up the nucleation process and slowing down the crystal growth. This is essential to obtain perovskite films with homogeneous and continuous morphologies. Uncontrolled fast crystallization leads to a morphology characterized by micrometric structures like needle growth by rod-shaped $PbI_2$ colloidal seeds,[40] with low uniformity and high density of voids that contribute to poor performance and shunting in the resulting devices.

The most common lab-scale deposition methods of perovskite from solution can be classified into two basic procedures: one-step and two-step coating (Fig. 4).

One-step coating consists of the deposition of the solution containing all perovskite precursors and then thermal annealing to remove the solvents and induce the crystallization process. In the two-step procedure, the precursors are deposited by separate solutions, coating first $PbI_2$ followed by $CH_3NH_3I$ properly solubilized in different solvents (for $MAPbI_3$-based perovskite), completed by the final thermal annealing step. Therefore, proper control and optimization of the deposition parameters is needed to obtain high-quality films and devices.

Several methods have been developed mainly to regulate the nucleation step and to control the overall crystallization process through (i) the optimization of the deposition process by introducing additional steps to facilitate and control solvent removal such as anti-solvent dripping/bath,[6,59] solvent annealing,[60–62] gas quenching,[63–65] flash IR annealing,[66] vacuum treatment;[67] (ii) precursor solution solvent engineering to trigger controlled supersaturated nucleation;[39] (iii) the use of functional additives, such as halide anion inducing the formation halo-plumbate species with different coordination degrees of $Pb^{2+}$ ions,[68] Lewis acid–base adducts[35] and molecular or polymeric additives[27,32,34,69] interacting with perovskite precursors; (iv) the substrate wettability modification through surface engineering[70] *etc.*

However, the intrinsic irreproducibility of most of these methods still limits their scalability, making the fabrication of good optoelectronic films with up-scalable techniques the next challenge to overcome for perovskite commercialization. With this aim, several polymeric materials have recently been explored to intervene in the control of the perovskite nucleation and crystallization process,[26] as reported in Section 3.

## 3. Polymer/perovskite composite as an active layer in solar cells: an overview

Among the different methods developed to control and guide the perovskite formation, the exploration of polymeric additives is of great interest, proving a successful approach to obtain

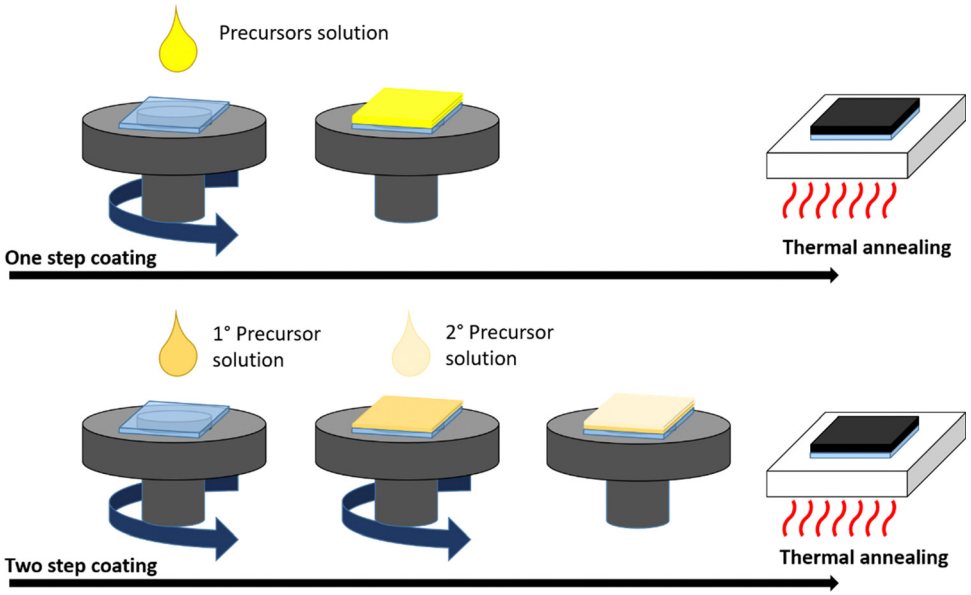


Fig. 4 Schematic description of one-step and two-step coating deposition.

high-quality active layers targeting optoelectronic control. The use of polymers has proven to be a viable strategy to overcome many of the challenges concerning perovskite materials, as schematized in Fig. 5. First, polymeric additives play an important role in delaying nucleation and precursor assembly processes to tune the kinetics of perovskite crystallization. This results in an easy modulation of perovskite crystallite size and morphology. Moreover, polymer macromolecules with a high molecular weight can remain in the film to form a composite, whereas other kinds of additives might evaporate during the annealing process. The polymer is usually located at the grain boundaries of perovskite films, from which moisture preferentially permeates and the degradation starts,[71] thus acting as a passivating/protecting agent that can improve PSC performance in a humid environment over time.[35] Selecting polymers with appropriate functional groups that can specifically interact with perovskite precursors results in enhanced efficiency and reduced degradation rates. In addition, polymers can mechanically reinforce fragile perovskite polycrystalline films, making them mechanically more robust to fracture processes.[31,72]

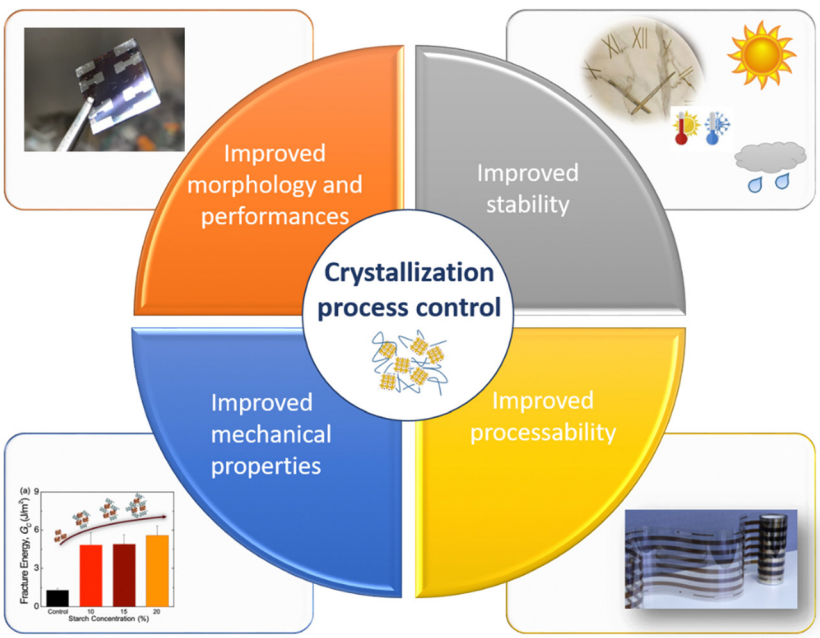


Fig. 5 Polymers as a new strategy to solve the major challenges related to metal halide perovskite materials reproduced from ref. 31,75 with permission from American Chemical Society, copyright 2022, and Cell Press, under a Creative Commons Attribution 4.0 International License (CC BY 4.0).

Table 1 List of polymers used as additives for the active layer of Perovskite-based solar cell

| Polymer | Molecular structure |
|---|---|
| Poly[2-methoxy-5-(2′ethylhexyloxy)-*p*-phenylene vinylene] (MEH-PPV)<br>Main properties: p-type semiconductor | 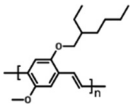 |
| Polymethyl methacrylate (PMMA)<br>Main properties: thermoplastic polymer, hydrophobic nature | 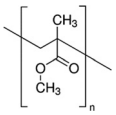 |
| Poly[(9,9-bis(3′-(*N*,*N*-dimethylamino)propyl)-2,7-fluorene)-*alt*-2,7-(9,9-dioctylfluorene)] (PFN)<br>Main properties: conjugated polyelectrolyte | 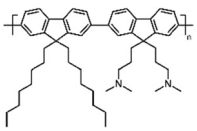 |
| Poly(triarylamine) (PTAA)<br>Main properties: p-type semiconductor | 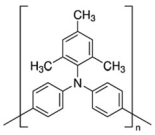 |
| Polyethylene glycol (PEG)<br>Main properties: hydrophilic nature, biocompatible, insulator | 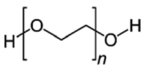 |
| Poly(4-vinylpyridine) (P4VP)<br>Main properties: hydrophobic nature | 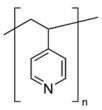 |
| Branched- polyethyleneimine (b-PEI)<br>Main properties: polyelectrolyte, adhesive properties | 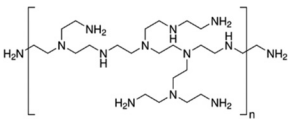 |
| Polyacrylic acid (PAA)<br>Main properties: hydrophilic nature | 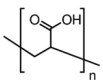 |
| Polyurethane (PU)<br>Main properties: elastomer | 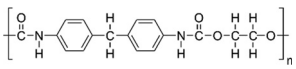 |
| Corn Starch (Maize)<br>Main properties: polysaccharide, hygroscopic nature, gelling properties, insulator biomaterial | 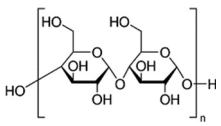 |
| Poly(styrene-*co*-butadiene)-polyurethane (SBS-PU)<br>Main properties: hard rubber (SBS) – elastomer (PU) | 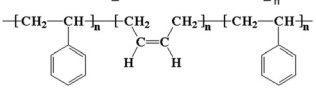 |
| | 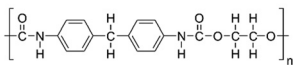 |
| Poly(ethylene glycol) tridecyl ether (PEGTE)<br>Main properties: hydrophilic nature | 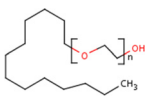 |
| Poly(propylene carbonate) (PPC)<br>Main properties: thermoplastic polymer, hydrophobic nature, polymeric Lewis base | 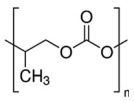 |
| Poly(vinyl alcohol) (PVA)<br>Main properties: hydrophilic nature, dispersants, flocculants, thickeners, biodegradable and water soluble | 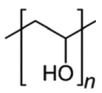 |
| Hydroxyethyl cellulose (HEC)<br>Main properties: polysaccharide, hydrophilic nature, gelling properties, insulator, biomaterial | 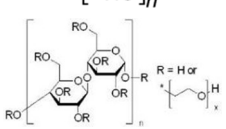 |
| 3D star-shaped polyhedral oligomeric silsesquioxane-poly(trifluoroethylmethacrylate)-*b*-poly(methylmethacrylate) (PPP) | |

Table 1 (*continued*)

| Polymer | Molecular structure |
|---|---|
| Main properties: 3D structure stability (rigid Si–O–Si); hydrophobic and anti-adhesion properties (Poly(trifluoroethyl methacrylate)) | 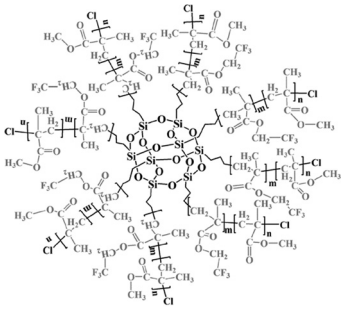 PPP |
| β-Poly(1,1-difluoroethylene) (β-pV2F)<br>Main properties: thermoplastic polymer, hydrophobic nature, polymeric Lewis acid | 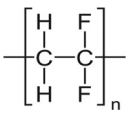 |
| *In situ* polymerized 3-fluoro-4-methoxy-4′,4″-bis((4-vinyl benzyl ether) methyl)) triphenylamine (FTPA)<br>Main properties: hydrophobic nature | 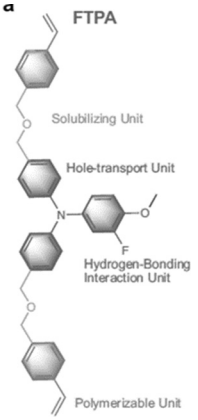 a FTPA Solubilizing Unit Hole-transport Unit Hydrogen-Bonding Interaction Unit Polymerizable Unit |
| Gellan Gum (GG)<br>Main properties: polysaccharide, hydrophilic nature, gelling properties, insulator, biomaterial | 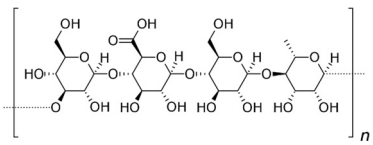 |

From a manufacturing perspective, polymers can imbue perovskite materials with simple processability, allowing the deposition of uniform and homogenous layers in a single printing step.[24,26,27,32,73,74]

Polymers can be classified according to their properties (*e.g.* hydrophilicity, thermo-plasticity, conductivity, *etc.*) and to their possible interaction with perovskite precursors and effects on PSCs.[26] The general criterion for selecting polymeric additives is to participate in perovskite crystallization so as to tune the perovskite film morphology, poly-crystal sizes, and passivation of grain boundaries.

The interest in polymer-perovskite based systems has increased, mainly aiming at correlating the chemical structure of the polymer and the resulting perovskite film properties. To date, fundamental material science investigations in the field have mainly focused on

(i) Impacts of the selected polymer on crystal growth and crystallization kinetics;

(ii) Influences of the perovskite/polymer film morphology on the optoelectronic properties;

(iii) Environmental stability and mechanical robustness of the perovskite/polymer films;

(iv) Simplified solution processability of the perovskite/polymer inks.

We therefore focus in this section on an in-depth analysis of the polymer influence on the perovskite, from the crystallization process to the final properties of the film and PSC performance, to better define the key points of the approaches reported in the literature.

In Table 1, we report a list of polymers used so far as additives in a perovskite active layer for solar cells based on the polymer structure. The effects induced by the polymer on the solar cell performance and the device architecture are also summarized in Table 2.

### 3.1. Influence of the polymer on hybrid halide perovskite: from the crystallization process to film optoelectronic properties

In 2015, Masi *et al.* reported the first work[30] on the use of polymers to control and guide the $MAPbI_3$ perovskite self-assembly through the interaction, already established in solution, between the

 

Table 2 List of the effects of the explored polymers on the perovskite solar cell performances and properties

| Polymer | | | Device performances | | | | | |
|---|---|---|---|---|---|---|---|---|
| ID | Concentration | Device architecture | $J_{SC}$ [mA cm$^{-2}$] | $V_{oc}$ [V] | FF | PCE [%] | Main influences PSC parameters | Year |
| PEG | 1–5% wt/wt$_{prec}$<br>Best 1% wt/wt$_{prec}$ | FTO/$TiO_2$/spiro-OMeTAD/$CH_3NH_3PbI_{3-x}Cl_x$/Au | 19.53 | 0.94 | 0.70 | 13.20 | – Slowing down the crystallization<br>– Substrate coverage improvement<br>– Morphology improvement | 2015[76] |
| PEG | 20–80 mg mL$^{-1}$<br>Best 20 mg mL$^{-1}$ | FTO/$TiO_2$/$MAPbI_3$/spiro-MeOTAD/Au | 22.50 | 0.98 | 0.72 | 16.00 | – Slowing down the crystallization<br>– Crystal growth template<br>– Morphology improvement<br>– Stability | 2016[34] |
| PMMA | 0.3–4 mg mL$^{-1}$<br>Best 0.6 mg mL$^{-1}$ | FTO/c$TiO_2$/m$TiO_2$/$(FAI)_{0.81}(PbI_2)_{0.85}$-$(MAPbBr_3)_{0.15}$/spiro-MeOTAD/Au | 23.70 | 1.14 | 0.78 | 21.60 | – Slowing down the crystallization<br>– Morphology improvement<br>– Defect passivation | 2016[33] |
| P4VP | Best 1 : 1000 by wt%$_{MAI}$ | ITO/$SnO_2$/$MAPbI_3$/spiro-MeOTAD/Au | 21.74 | 1.15 | 0.81 | 20.23 | – Defect passivation<br>– Stability | 2017[77] |
| b-PEI | | | 21.94 | 1.07 | 0.71 | 16.67 | – High binding energy with $Pb^{2+}$ | |
| PAA | | | 21.53 | 1.16 | 0.79 | 19.65 | – Defect passivation | |
| PU | 0.01–0.1 wt%<br>Best 0.02 wt% | ITO/NiOx/$MAPbI_3$/PCBM/BCP/Ag | 22.12 | 1.05 | 0.80 | 18.7 | – Slowing down the crystallization<br>– Morphology improvement<br>– Defect passivation<br>– Stability<br>– Mechanical improvement | 2017[78] |
| Maize | 5–20% wt/wt$_{prec}$<br>Best 10% wt/wt$_{prec}$ | ITO/Poly-TpD/$MAPbI_3$/$PC_{61}BM$<br>BCP/Al | 21.9 | 1.10 | 0.78 | 18.8 | – Slowing down the crystallization<br>– Crystal growth template<br>– Morphology improvement<br>– Stability<br>– Mechanical improvement | 2018[27,31,74] |
| SBS-PU | 0.02–0.08 wt% $C_{PU}$<br>0.3–1.2 mg mL$^{-1}$ $C_{SBS}$<br>Best 0.04 wt%–0.6 mg mL$^{-1}$ | ITO/$NiO_x$/$MAPbI_3$/PCBM/BCP/Ag<br>PDMS/PEDOT:PSS Perovskite/PEI/PEDOT:PSS/PDMS | 22.60<br>18.70 | 1.12<br>1.07 | 0.80<br>0.78 | 20.25<br>15.61 | – Slowing down the crystallization<br>– Morphology improvement<br>– Defect Passivation<br>– Stability<br>– Mechanical improvement | 2019[72] |
| PEGTE | 0–0.3 wt%<br>Best 0.07 wt% | ITO/$NiO_x$/MAPbI3/$PC_{61}BM$/BCP/Ag | 19.61 | 1.08 | 0.79 | 16.96 | – Slowing down the crystallization<br>– Crystal growth template<br>– Defect passivation | 2019[79] |
| PPC | 0.1–5 wt%<br>Best 0.3 wt% | ITO/$SnO_2$/$MAPbI_3$/spiro-MeOTAD/Ag | 22.81 | 1.13 | 0.78 | 20.06 | – Slowing down the crystallization<br>– Crystal growth template<br>– Defect passivation | 2019[35] |
| PVA | 1–5 mg mL$^{-1}$<br>Best 3 mg mL$^{-1}$ | ITO/PEDOT:PSS/$FASnI_3$/C60/BCP/Ag | 20.37 | 0.63 | 0.69 | 8.92 | – Slowing down the crystallization<br>– Morphology improvement<br>– Retarding the $Sn^{2+}$ oxidation<br>– Stability | 2019[80] |
| PEG | 80 mg mL$^{-1}$ | FTO/mp$TiO_2$/$CsPbBr_3$/Carbon | 7.56 | 1.41 | 0.73 | 7.8 | – Increasing the nucleation rate<br>– Morphology improvement<br>– Stability | 2020[81] |
| HEC | 2.5% wt/wt$_{prec}$ | ITO/Poly-TpD/$MAPbI_3$/$PC_{61}BM$/BCP/Al | 17.9 | 1.12 | 0.78 | 15.7 | – Slowing down the crystallization<br>– Crystal growth template<br>– Morphology improvement<br>– Stability | 2021[32] |
| PPP | 0–1.0 mg $mL_{antisolvent}^{-1}$<br>Best 0.1 mg mL$^{-1}$ | ITO/NiOx/perovskite/PCBM + C60/BCP/Cr/Au | 23.24 | 1.13 | 0.84 | 22.1 | – Regulation of crystallization<br>– Defect Passivation<br>– Inhibit nonradiative recombination and charge-transport loss<br>– Stability | 2022[82] |
| β-pV2F | 0.5 mg mL$^{-1}$ | ITO/MeO-2PACz/$Cs_{0.05}(FA_{0.98-MA_{0.02}})_{0.95}Pb(I_{0.98}Br_{0.02})_3$/PC61BM/BCP/Ag | 24.8 | 1.18 | 0.84 | 24.6 | – Suppression of intermediate DMSO-DMF-PbX2 phase<br>– Reduction of the black perovskite phase formation energy, promoting phase conversion and crystalline order<br>– Suppression of Ion migration and interfacial charge extraction<br>– Stability | 2023[28] |
| FTPA | 5% molar ratio/prec | FTO/CBD-$SnO_2$/perovskite-FTPA/FTPA/Spiro-OMeTAD/Au | 24.4 | 1.18 | 0.83 | 24.1 | – Slowing down the crystallization<br>– Inhibit nonradiative recombination and charge-transport loss<br>– Stability | 2023[36] |
| GG | 12 mg mL$^{-1}$ | ITO/PTAA/4FPEAI/$MAPb(I_{1-x}Br_x)_3$ $x$ = 0.1/PC61BM/BCP/Ag | 20.95 | 1.09 | 77 | 17.69 | – Crystal growth template<br>– Morphology improvement<br>– Improved light stability | 2023[83] |

precursors and the chemical groups present in the molecular chain by acting as a template to obtain a smooth morphology film in a single step deposition. They explored several commercial semiconductor polymers and proposed the p-type poly[2-methoxy-5-(2-ethylhexyloxy)-1,4-phenylenevinylene] (MEH-PPV) as suitable. However, the implementation of the composite as an active layer into a solar cell showed a low maximum PCE of ~3%, due to the charge/transfer mechanism occurring at the $MAPbI_3$/semiconducting polymer interface that hindered efficient charge extraction because of the very different charge mobility characterizing the perovskite and polymer domains. Following this first pioneering results, the interactions occurring in solution between perovskite $MA^+$ precursors and polymer functional groups were rationalized by the systematic investigation of five polymers: MEH-PPV, poly(methyl methacrylate) (PMMA), poly[(9,9-bis(3′-(*N*,*N*-dimethylamino)propyl)-2,7-fluorene)-*alt*-2,7-(9,9-dioctylfluorene)] (PFN), 2,4-dimethyl-poly(triarylamine) (PTAA), and polystyrene (PS). The nature of chemical interactions with perovskite precursors was explored using NMR spectroscopy.[29] The study demonstrated that establishing hydrogen bond interactions between $MA^+$ cation and polymers in solution is fundamental for the polymer to guide the self-assembly process of perovskite crystals for high-quality films, as shown by correlation with atomic force microscopy (AFM) and scanning electron microscopy (SEM).

Then, the influence of polymers characterized by different functional groups on the crystallization process was investigated, by correlating it with the conditions of deposition. Indeed, the perovskite crystallization is driven by the supersaturation of the solution, the control of which is crucial to obtain a uniform morphology, as previously described. Since the method of film deposition and formation affects the morphology and then the optoelectronic properties of the MHP film, the effective role of the polymer can be better understood by distinguishing two main deposition conditions: one-step fabrication without and with antisolvent dripping. In the first case, the role of the polymer is crucial for controlling the crystallization process, while in the second case, there is a cooperative contribution of antisolvents and polymers, which, however, does not play a major role in controlling the process.

**3.1.1. Polymer-assisted one step dripping free deposition.** This section summarises the most interesting studies on the deposition of perovskites in one step, antisolvent-free, which represents the method in which the contribution of the polymers in driving crystallization is most evident, as there is no contribution from dripping to control the supersaturation of the solution.

Among the first studies on the use of polymer to guide the perovskite self-assembling, in 2015, Chang *et al.*[76] explored the effect of an insulating polymer PEG, observing that by adding 1 wt% respect to the precursors, the wettability onto the substrate was improved, leading to better and more uniform coverage in one step deposition, as evidenced by SEM analysis. Moreover, these authors speculated that the presence of PEG contributes to retard the crystallization process of the perovskite, resulting in a continuous film with adequate domain sizes and reduced voids between perovskite domains. This prevented direct contact between $TiO_2$ and the HTL, increasing the open circuit voltage ($V_{oc}$) to 0.97 V, as well as the $J_{SC}$ (19.53 mA $cm^{-2}$) and the FF (0.7), showing a PCE of 13.2%. They also observed that higher PEG concentration increases the film roughness and decreases device performance due to the insulating properties of the polymer. Based on the previous results, a novel MAPbI3 perovskite solar cell architecture based on an insulating polymer scaffold structure was developed by Zhao *et al.*[34] who replaced the inorganic nanocrystal-based mesoporous scaffold with a long- and flexible-insulating polymer chain PEG-based network. The first direct impact of their approach was on the decrease of the temperature process down to 105 °C with respect to the high temperatures (>450 °C) used for sintering inorganic metal oxide, simplifying and reducing the cost of the process. As a three-dimensional skeleton, PEG guides perovskite assembly, slowing down the crystallization, as evidenced by the different time evolution of the intermediate phase analysed by X-ray diffraction analysis. This in combination with the improved wettability of the precursor solution after introducing PEG, results in the formation of a uniform high-quality morphology film characterized by dense perovskite crystalline grains surrounded and 'cross-linked' by amorphous polymer material (as shown in Fig. 6(a)). Among all the explored molecular weights, values >20 000 Da showed the best performance because longer PEG molecules allow better control of the formation of a three-dimensional network favouring the formation of a film with uniform morphology, achieving the highest PCE of 16% with a $V_{oc}$ of 0.98 V, a $J_{SC}$ of 22.5 mA $cm^{-2}$, and a FF of 0.72. These were among the first studies demonstrating the important role of the PEG scaffold in driving the perovskite crystallization in one-step antisolvent-free deposition, resulting in a high-quality morphology film. In addition, the presence of the interconnected PEG scaffold in the perovskite film, despite its insulating nature, does not interfere with the charge harvesting and transport in the active layer, leading to improved photovoltaic performances.

In 2018, Giuri *et al.*[27] started a study on the influence of the biopolymer starch from maize on several aspects concerning perovskite materials, from interaction in solution with precursors to crystallization process, environmental and thermomechanical stability and processability. The –OH groups present on the long molecular chains of the polymer interact with methylammonium iodide of perovskite precursors in solution, forming a persistent sol–gel network as shown by the GIWAXS analysis in Fig. 6(b). Moreover, the rheological investigation of the perovskite precursor solutions, with different polymer/precursor ratios, showed an interesting tunability of the rheological behaviour of the ink.[74] The cooperative presence of the two previous conditions influences and drives the crystallization process of the perovskite, deposited in a single-step coating (antisolvent dripping free), by delaying it.[41] This allows better control of film formation in a uniform and high-quality morphology characterized by increased grain size, with the polymer homogeneously distributed around the grain boundaries, acting as a reinforcement and enhancing the thermodynamic stability of the maize-perovskite composite. The as-developed

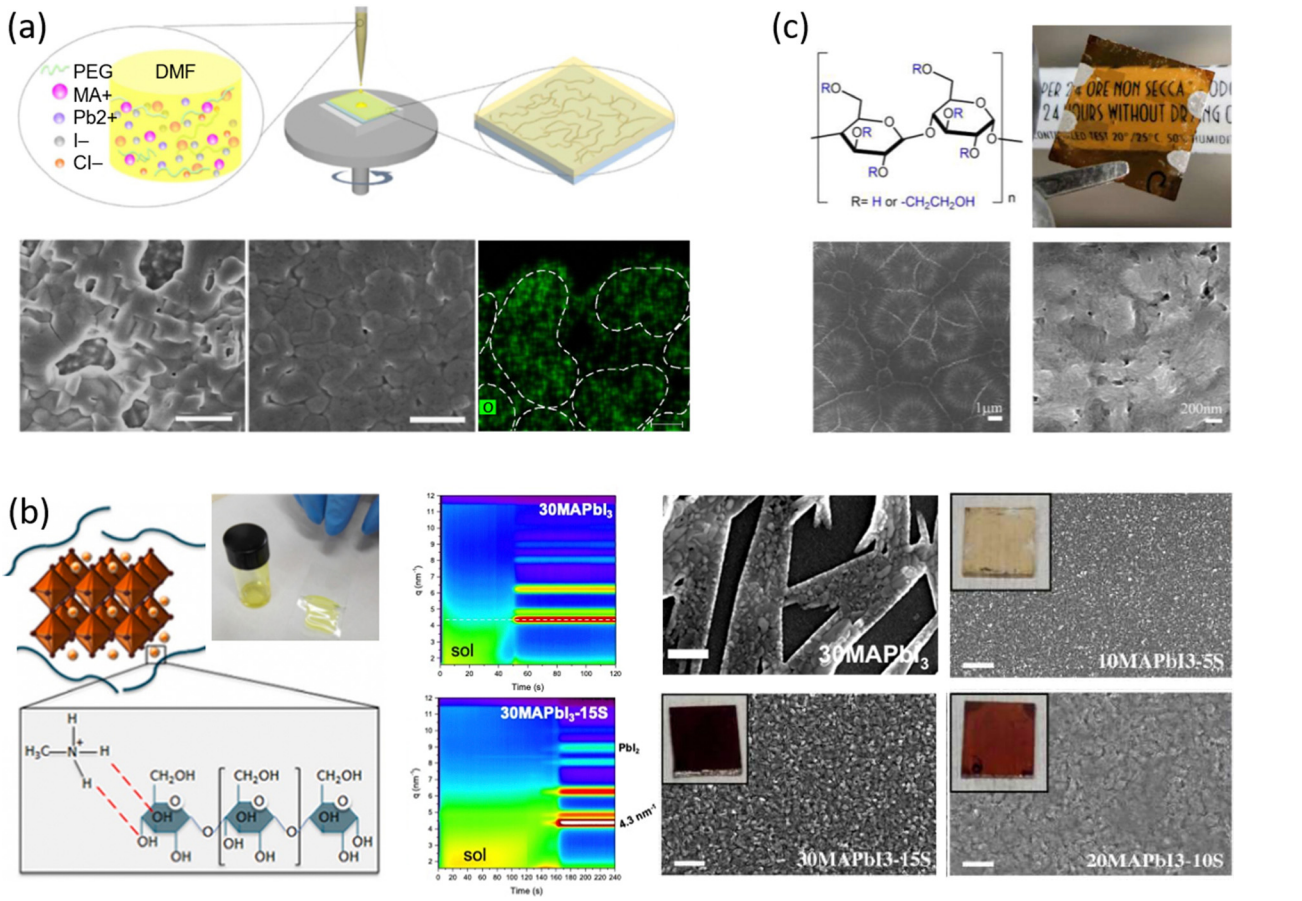


Fig. 6 Effect of polymers on perovskite crystallization and film morphology in one step dripping free deposition assisted by (a) PEG from DMF based precursor solutions: a sketch of the one-step fabrication process of perovskite film with polymer scaffold, SEM of the perovskite films without and with PEG. (Scale bar, 1 μm), EDS mapping of O element of the perovskite-PEG film corresponds to PEG distribution (Scale bar, 10 nm), reproduced from ref. 34 with permission from Springer Nature, copyright 2016 under a Creative Commons Attribution 4.0 International License (CC BY 4.0); (b) Corn starch from DMSO based precursors solutions: sketch of the hydrogen bonding interaction between the starch molecules and the MAI of the perovskite precursors with the photo of the gel-like behaviour of the 30MAPbI3-15S solution, 2D intensity maps during film formation from the perovskite precursor solution without (30MAPbI3) and with starch (30MAPbI3-15S), SEM images of starch/perovskite film by varying the perovskite precursor with the respective photo in the inset, reproduced from ref. 27,41 with permission from Elsevier, copyright 2018, and IOP Publishing, copyright 2021; (c) HEC from DMSO based precursor solutions: 2-hydroxyethyl cellulose molecular structure, digital photos of a semi-transparent device, low and high magnification SEM of a MAPbI3-HEC film, reproduced from ref. 32 with permission from Elsevier, copyright 2021.

composite implemented in the photovoltaic devices shows a very high PCE of 18.8% ($J_{SC}$ = 21.9 mA cm$^{-2}$, $V_{oc}$ = 1.10 V and FF = 0.78) despite the insulating nature of the maize, with very high reproducibility. Moreover, time-resolved photoluminescence (TRPL) measurements showed a slight improvement in charge carrier lifetime indicating that surface recombination was likely mitigated by the polymer, that surrounding the grain boundaries ensures adequate charge transport through the perovskite grains.[31,84] In addition, the thickness of the final film can be easily tuned by varying the viscosity of the solution, allowing the properties of the ink and thus the film to be adapted to the final application, further validating the developed approach.[27,32,85,86]

Besides interfering with the film formation, transparent and insulating polymers can also improve the transmittance of perovskite composite materials. To this end, hydroxyethyl cellulose (HEC) biopolymer inclusion in $MAPbI_3$ was exploited by Bisconti *et al.* in 2021 to manage transparency and to improve thermal stability of perovskite materials for application in smart windows.[32] The hydroxyl and hydroxyethyl groups, characteristic of the HEC macromolecule, interact with the perovskite precursors in solution, which in combination with the gelling properties of the HEC in DMSO results in the formation of a compact and uniform perovskite film characterized by the Liesegang ring, as shown in Fig. 6(c). These structures indeed are typical of crystallization occurring when nucleating particles induce a drop in the super saturation levels of their surroundings, as in gels that prevent the convection and sedimentation of the nuclei, which could hinder the formation of such rings, leading to the formation of spacing regions between nucleation centres.[87] In detail, we observed these characteristic structures, at low magnifications, in most of the perovskite films made from DMSO solution by one-step (antisolvent-free) polymer-assisted deposition, especially when the polymer influences the viscosity.

Regarding the $MAPbI_3$-HEC composite, by simply varying the polymer/precursor ratio, it was possible to tune not only the morphology but also the thickness and the average transmittance (AVT) of the active layer, obtaining a good compromise between solar cell transparency and performance. The implementation of the composites in the active layer of solar cells showed the best PCE of 15.7% with an AVT of 27% for a layer thickness of 220 nm, without hysteresis. The device stability to thermal stress was also improved, as detailed in Section 2.2, which is important for the future application of these devices in building integrated photovoltaics.

Recently, mixed halide perovskite with tunable wide band gap ($MAPb(I_{1-x}Br_x)_3$) was developed by Bisconti *et al.*[83] *via* polymer-mediated crystallization assisted by Gellan gum. A homogenous morphology with large and compact perovskite grains was obtained, without any solvent dripping, responsible for the improvement in the $V_{oc}$ values of the photovoltaic device, compared to the reference perovskite. The overall photovoltaic parameters are similar to the performance of the perovskite, due to the reduction in FF and $J_{SC}$ attributed to the insulating nature of the GG polymers. In this case, the photostability of the perovskite was improved by the presence of the polymer, as discussed later, in the relevant section.

#### 3.1.2. Antisolvent dripping-polymer assisted deposition

*Polymers added to the precursor solution.* Differently from the deposition method previously described, the fabrication involving the intermediate step with antisolvent dripping allows for control over the supersaturation process accelerated by the use of antisolvent, which is in addition to the contribution of the polymer on the control of perovskite crystallization.

Another significant difference from the previous method is the amount of polymer added into the solution, which is very small; indeed, it can be considered an additive to improve film properties. These aspects imply that the deposition conditions (*e.g.*, solvents, fabrication parameters) are not changed too much from those of the reference perovskite, so it is the most popular approach among authors.

Huang *et al.* investigated the inclusion of Polyurethane (PU) elastomer into $MAPbI_3$ perovskite with the aim of both delaying the crystallization rate and improving the stability and flexibility of the film.[78] XPS and FTIR analyses demonstrated that PU interacts with $Pb^{2+}$ through strong chelation, retarding the crystallization rate and favouring the formation of a compact and homogeneous film with highly crystallized, large micrometre size grains, as shown by XRD and SEM analyses. The implementation of the active film into the photovoltaic device showed a PCE of 18.7% with a $J_{SC}$ of 22.12 mA $cm^{-2}$, without photocurrent hysteresis, revealing (by PL measurements) superior electronic quality and a reduced defect concentration consistent with a high $V_{oc}$ of 1.05 V and a FF of 80.3%.

To regulate the crystallization kinetics of perovskite, PEG-based additive, poly(ethylene glycol) tridecyl ether (PEGTE), was tested by Hong *et al.*[79] in 2019. A very small amount of polymer (0.07 wt%) improved the efficiency of the device by up to 16.96%, by increasing $J_{SC}$ and FF to 19.61 mA $cm^{-2}$ and 0.79 respectively, while $V_{oc}$ is kept unchanged if compared to $MAPbI_3$. The improved performance is attributed to several reasons. From the analysis of the influence of annealing-time on device performance, the authors claimed that the polymer coordinates with the perovskite precursors, most likely with $PbI_2$ *via* the hydroxyl group, slowing down the crystallization speed, allowing the defect sites in the film to be reduced. Indeed, from SEM and AFM analyses, the morphology of the film containing the additive appears pinhole-free and smooth allowing the suppression of charge recombination both between free charges and between trapped and free ones, improving electrical stability under continuous illumination.

One of the most effective polymers, explored in 2019 by Han *et al.*,[35] is PPC, a linear copolymer of carbon dioxide and propylene oxide, characterized by carbonate groups with a high molecular dipole moment that, as a Lewis base, interacts with the Lewis acidic perovskite precursors of $MAPbI_3$, *i.e.*, the methylammonium cations ($CH_3NH_3^+$) and iodoplumbate anions to form a strong and stable Lewis acid–base adduct. This stronger Lewis acid–base interaction allows the crystallization of the perovskite to be controlled, by increasing the activation energy for nucleation and the diffusion of the precursor molecules, decreasing the number of nuclei, and slowing down crystal growth. The enlarged grain size grows until it reaches the surrounding long-chain polymer, merging with the other grain and interconnecting *via* cross-linking as schematically detailed in Fig. 7(a). This inter-grain bridge minimizes inter-grain electrical decoupling due to the remnant polymeric Lewis bases that can donate lone pairs electrons from the oxygen atom to coordinate with perovskite crystal defects such as $Pb^{2+}$ or $NH^{3+}$ at the grain boundaries, thus passivating the defect site. Improved and more stable performance, with a PCE of 20.06% ($J_{SC}$ = 22.81 mA $cm^{-2}$, $V_{oc}$ = 1.13 V, FF = 0.77) was achieved with the nanocomposite.

In 2019, the approach of polymeric additive was also extended to lead-free $FASnI_3$ perovskites by Meng *et al.*[80] with the aim to solve one of the main issues related to the formation of a perovskite film with poor coverage and numerous pinholes, due to a fast self-assembly process, generating a number of trap states that degrade the device performance. The inclusion of a polymer, poly(vinyl alcohol) (PVA), characterized by a high density of hydroxyl groups that can establish strong $O–H\cdots I^-$ hydrogen bonding interactions with FA (as observed by liquid-state $^1H$ NMR measurements), was found to speed-up nucleation and slow down crystal growth, eventually obtaining a compact and pinholes free perovskite film, with reduced grain size (100–300 nm) (Fig. 7(b)). This, along with the reduced trap states at the grain boundaries and the suppressed iodide ion migrations, and the antioxidant property of the hydroxyl groups in PVA (following their oxidation to aldehydes or carboxylic acids, contributes to reduce $Sn^{2+}$ oxidation), allowed for the achievement of a PCE of 8.92% and improved long-term stability.

Another issue that has been attempted to be solved by the use of polymers as additives concerns the control of FA-based perovskite crystallization and the stabilization of the highly ordered black perovskite phase.

With this goal, in 2023, Li *et al.* investigated the dipolar structure of b-poly(1,1-difluoroethylene).[36] Specifically, the

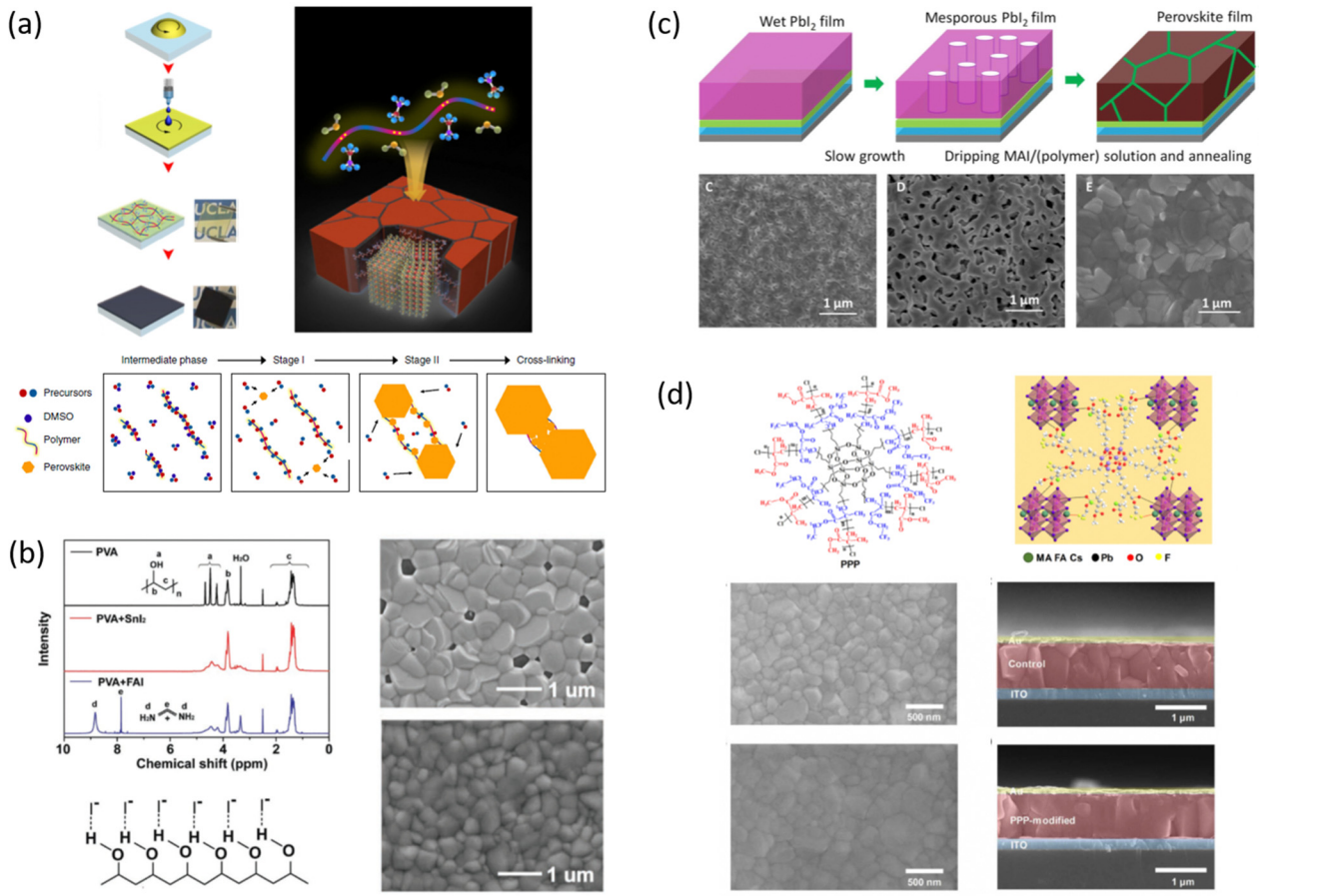


Fig. 7 Effect of polymers on perovskite crystallization and film morphology in one step dripping assisted deposition. (a) Step of fabrication of PPC-perovskite films along with a schematic illustration of the perovskite grain growth and inter-grain cross-linking induced by the macromolecular intermediate phase, reproduced from ref. 35 with permission from Springer Nature, copyright 2019 under a Creative Commons Attribution 4.0 International License (CC BY 4.0); (b) hydrogen bonding interaction in solution between FASnI3 based perovskite precursors and PVA, SEM morphology of perovskite without (top) and with PVA, reproduced from ref. 80 with permission from Wiley, copyright 2019; (c) schematic diagram of the developed interdiffusion method for incorporating the polymer into the perovskite films along with SEM images of a homogeneous $PbI_2$ film without slow growth, a mesoporous $PbI_2$ film with slow growth, and a perovskite film processed from slowly grown PbI2 with PVP polymers, reproduced from ref. 77 with permission from the American Association for the Advancement of Science, copyright 2017 under a Creative Commons Attribution 4.0 International License (CC BY 4.0); (d) Structural formula of the PPP polymer and sketch of the interaction between the PPP polymer (partial 3D structure) and perovskite, SEM images of the control and PPP-modified perovskite films with respective cross-section, reproduced from ref. 82 with permission from American Association for the Advancement of Science, copyright 2021 under a Creative Commons license.

polymer acts as a Lewis acid due to the all-trans planar zigzag conformation with the electron-withdrawing effect of the fluorine atoms inducing a partial positive charge density on the neighboring hydrogen atoms. The C–H···X dipole interaction between $-CH_2$ and the halide ions of $[PbX_6]^{4-}$ of the perovskite influences crystallization by reducing the formation energy of the black photoactive phase and controls the formation of a low-defect crystalline perovskite film improving solar cell performance. In addition, this polar interaction increases the surface work function (WF) after film formation facilitating the interfacial charge extraction. They achieved a certified PCE of 24.2% on an active area of 9.6 $mm^2$ ($V_{oc}$ = 1.17 V, FF = 0.83). The fluorine groups exposed from the surface also enhance the hydrophobicity, then the stability of the film.

Even the all-inorganic perovskite $CsPbBr_3$-based film, although shows superior stability with respect to the other compositions, suffers from poor morphology, impurity phase and defects due to unbalance between slow nucleation and fast growth during the crystallization process. With the aim to improve the quality of the film, in 2020 Ren *et al.*[81] explored the use of PEG to regulate the nucleation kinetics of $CsPbBr_3$ in one-step dripping-assisted deposition. They observed that the Lewis base of PEG interacts with the Lewis acid of $Pb^{2+}$ reducing the size of the CsBr-$PbBr_2$-DMSO colloids and increasing the density of nuclei, promoting faster heterogeneous nucleation. The resulting optimized film showed a uniform and dense morphology characterized by small crystals. The improved film morphology characterized by a well-interconnected network, showed enhanced photovoltaic performance, with a PCE of 7.8% and a higher $V_{oc}$ of 1.41 V (FF = 0.73, $J_{SC}$ = 7.56), and improved UV stability.

Li *et al.* designed a multifunctional 3-fluoro-4-methoxy-4′,4″-bis((4-vinyl benzyl ether) methyl)) triphenylamine (FTPA)

molecule characterized by four main components: triphenylamine in the core that improves hole transport and regulates the energy levels in the bulk and surface of the perovskite film; end-groups of fluorine and oxygen atoms that interact with perovskite promoting the orientated crystallization of α-$FAPbI_3$ by restraining the generation of a multiintermediate phase; the flexible diethyl ether groups that act as a solubilizing unit; the vinyl terminal groups act as *in situ* for polymerization and stabilize α-$FAPbI_3$ by filling the grain boundaries of perovskite as a hydrogen-bonding network.[36] In detail, the strong hydrogen-bonded interaction between the fluorine and oxygen atoms of FTPA led to the formation of the intermediate phase FTPA-FAI-$PbI_2$ by restraining the other intermediate phases of $MA_2Pb_3I_8{\cdot}2DMSO$ and δ-$FAPbI_3$, and increases the energy barrier for perovskite nucleation, retarding the crystallization kinetics, resulting in high crystal quality. The FTPA also acts as a bridge between the perovskite grains, minimizing electrical decoupling and inhibiting nonradiative recombination. The best device configuration based on *in situ* polymerized FTPA shows a PCE of 24.1% ($V_{oc}$ = 1.18 V, $J_{SC}$ = 24.43 mA $cm^{-2}$, FF = 83.45) and excellent illumination, moisture, and thermal stability.

*Polymers added into the antisolvent dripping.* Several authors included the polymers into the perovskite through the antisolvent, during the deposition step to overcome the solubility issues taking place during the mixing with the precursor solutions.

In 2016, Bi *et al.* explored the influence of poly(methyl methacrylate) (PMMA) to control mixed cation perovskite crystallization.[33] In detail, the polymer was introduced during the dripping of the spin coating process, with the aim of controlling crystal formation and growth. As revealed by FTIR, the carbonyl groups of PMMA form an intermediate adduct with $PbI_2$, which slows down the crystal growth allowing the formation of random nuclei that favour heterogeneous nucleation. This determines the formation of a smooth perovskite film with improved grain size growing in a thermodynamically preferred direction, to minimize the total Gibbs free energy of the system. The smooth and shiny films based on the PMMA-perovskite composite showed superior electronic quality due to the reduced defect concentration evidenced by PL and XPS analyses. This allowed the fabrication of perovskite solar cells with a PCE of up to 21.6%, using an antisolvent assisted method.

Zuo *et al.*,[77] in 2017, investigated the interaction with the perovskite film of three polymers characterized by different functional groups: branched polyethyleneimine (b-PEI) rich in (possibly protonated) amino groups, poly(4-vinylpyridine) (P4VP) rich in Lewis base pyridine groups, and Polyacrylic acid (PAA) rich in carboxylic acid groups due to the strong interactions between the polymers and the perovskite precursors, making it difficult to form a homogeneous film, the authors explored a new deposition method, called 'interdiffusion method', consisting in the formation of a mesoporous $PbI_2$ layer on which a solution of MAI/polymer in isopropanol was dripped leading to the formation of a perovskite film after infiltration and thermal annealing (Fig. 7(c)) without modify the morphology and crystallinity of the perovskite. The best performances (PCE = 20.23%) were obtained with the perovskite containing the pyridine group, having a binding energy of 37.70 kJ $mol^{-1}$ with $Pb^{2+}$. The authors concluded that the binding interaction between the perovskite and the polymers represents the key parameter affecting the passivation of the film, and then the performance of the device.

In 2019, inspired by nacre, a biomimetic crystallization approach was developed by the addition of an antithetic insoluble poly(styrene-*co*-butadiene)- soluble polyurethane (SBS-PU) composite matrix into perovskite.[72] In this work, Hu *et al.* observed a synergistic beneficial effect to the crystallization process: on the one hand, SBS reduced the number of nucleation sites, promoting heterogeneous nucleation; on the other hand, the interaction between PU and $PbX_2$ retard the crystallization, allowing the formation of a high quality and mechanical robust perovskite film with enhanced crystallinity, smoothness, and grain size (showing preferential perpendicular growth as micro parallel structures). Based on this method, the authors fabricated rigid and wearable perovskite-composite solar cells with maximum PCEs of 20.25% ($J_{SC}$ = 22.6 mA $cm^{-2}$, $V_{oc}$ = 1.12 V and FF = 0.80) and 15.61% ($J_{SC}$ = 18.7 mA $cm^{-2}$, $V_{oc}$ = 1.07 V and FF = 0.78), respectively.

Cao *et al.* designed an innovative 3D star-shaped polyhedral oligomeric silsesquioxane-poly(trifluoroethyl methacrylate)-*b*-poly(methylmethacrylate) (PPP) polymer to control perovskite film crystallization.[82] The multifunctional PPP polymer is based on a highly symmetrical rigid Si–O–Si cubic cage skeleton in the core, which confers stability to the structure, linked to polymeric branches of Poly(trifluoroethylmethacrylate) that exhibits outstanding hydrophobic and anti-adhesion properties to the film. PPP has multiple chemical anchor sites including C═O that strongly interact with $PbI_2$ and $-CF_3$ interact with $FA^+$ and $MA^+$ through hydrogen bonding (as shown in Fig. 7(d)), promoting the crystallisation of a high-quality film. Moreover, non-radiative recombination and charge transport loss are inhibited in the PPP-modified inverted devices, achieving a PCE of 22.11% ($V_{oc}$ = 1.13 V, $J_{SC}$ = 23.24 mA $cm^{-2}$, FF = 0.84) with improved stability under moisture, thermal, and illumination stress.

### 3.2. Influence of the polymer on perovskite stability

Improving the long-term chemical and thermomechanical stability of perovskite solar cells is the next technological challenge to be faced before commercial deployment of the technology. Identifying the degradation factors and mechanisms represents the key point for developing reliable perovskite materials, especially under operational conditions.[88–91]

Various strategies have been developed to improve perovskite stability:[31]

(1) Extrinsic reinforcement, based on the introduction of scaffold-based support,[92] through an additional step during fabrication or *via* encapsulation with different materials;[93]

(2) Intrinsic reinforcement, based on perovskite material engineering by tuning the composition or through the addition

of molecular or polymeric additives to stabilize and protect the perovskite from degradation.[27,48,69,86,94,95]

The use of polymeric additives to prevent perovskite film decomposition, in most cases, represents a successful solution to improve its stability to light, heat, and moisture-based chemical degradation.

First, as discussed in the previous section, because the polymer allows the control of the crystallization process of the perovskite, improving the morphology of the film and making it more compact and void-free, thus less available to the infiltration of external degrading agents, with beneficial consequences on the stability of the structure. In addition, the presence of polymer in the film, homogeneously distributed around the perovskite grains, and the different interactions of the polymer with the environment, especially in cases where the concentration of the polymer is significant, can provide a shield against the degrading effects of external factors, improving the stability of perovskite.

As an example, the hygroscopic nature of the long-chain maize network stabilizes and protects the polymer/perovskite from decomposition in an ambient environment. In detail, the unencapsulated devices containing maize tested in an ambient air of ~22 °C and a moisture content of 40–70%, according to the ISOS-D-1 protocol, showed a retention of 50% of initial PCE after about 400 h of aging test, with respect to the control device, showing a complete degradation just after 145 h.[27]

The maize-$MAPbI_3$ films showed enhanced thermodynamic stability as well, as demonstrated by evaluating the impact of thermal cycling at 85 °C (ISOS-T-1I) on device performance. Maize polymer indeed surrounds the perovskite grains and prevents the physical loss of the volatile methylammonium cation and the diffusion of the iodine species, thereby delaying the perovskite decomposition rate and improving the overall thermal stability of the active material. The stability of solar cells based on the composite material was also tested in the operational condition by tracking the current density at the maximum power point (MPP) under light cycling test (Fig. 8a), mimicking the diurnal sun-dark cycle (8-hour light/16 hours dark, ambient air $T$ ~25 °C, RH ~50%), according to the ISOS-LC-1 protocol. The inclusion of maize into the active layer also contributes to improving the photo-stability of the device in the presence of humidity, possibly due to the improved interface stability and reduced ion migration and defect formation caused by moisture. This was confirmed by the slower degradation of $V_{oc}$ and the stable FF, if compared to standard perovskite.[31]

The inclusion of a similar biopolymer, HEC, in $MAPbI_3$ also confers improved resistance to thermal degradation.[32] An in-depth analysis was conducted on the actual solar cells, by testing performance during thermal aging cycles at 85 °C, and on the HEC-perovskite film, aged under the same conditions, evaluating the influence of heat on morphological and structural properties (Fig. 8b). The devices containing HEC showed a PCE of around 74% of the initial value after 10 thermal cycles, unaltered $V_{oc}$, and a negligible reduction of the FF, if compared to ~48% of the initial PCE for standard perovskite. These data evidence improved tolerance to thermal stress in the presence of HEC due to the formation of clear interfaces and low series resistances to charge extraction in the device, as also confirmed by a more compact and uniform film morphology than aged standard $MAPbI_3$. A complete thermal characterization by TGA/DSC analysis demonstrated that the inclusion of HEC into the perovskite material delayed the loss of MAI under thermal stress and increased the activation energy of MAI sublimation, which is responsible for perovskite decomposition confirming the improved thermal stability conferred by the polymer.

Another strategy to improve the moisture tolerance of perovskite films is the use of hygroscopic polymers. The strong hygroscopicity of PEG molecules, together with their strong interaction with perovskite, improves the stability of the film in the presence of a highly humid environment (70% RH), showing an excellent unsealed device resistance for over 300 h.[34] The presence of a PEG scaffold around perovskite grains can absorb the water molecules creating a moisture barrier that protects the film from degradation. As we previously discussed in Section 1.2.1, the perovskite-PEG-based films and devices showed strong self-healing or water-resistance under vapor spray (Fig. 8c). After being vapor-sprayed, the film changed first from black color to light yellow, but, as evidenced by NMR measurements, the MAI molecules remain anchored by the PEG, and this allows the rapid recovery of the original $MAPbI_3$ phase after removal of the water source. This very fast decomposition-regeneration mechanism is due to the strong interaction between MAI and PEG polymers.

The inclusion of hydrophobic and thermoplastic PPC polymer was also found to be beneficial for perovskite stability in the presence of moisture (70 ± 5% RH for 150 h), light (one-sun for 2 h), and heat (100 °C for 66 h in $N_2$).[35] As evidenced by XRD analysis (Fig. 8d), in all three stress conditions, the perovskite containing PPC showed retarded degradation of the film, even more evident with an increasing amount of polymer. In contrast, the bare perovskite film showed a severe degradation to $PbI_2$ in each case, demonstrating the improved environmental stability induced by the hydrophobic and inter grain cross-linker PPC. Further confirmation was given by testing the stability of unencapsulated solar cells in an ambient environment for 1008 h, showing a constant PCE for the devices containing PPC compared to a degradation of about 64% for the bare perovskite. The stability of encapsulated devices under continuous illumination (90 ± 10 mW, without UV filter) and open-circuit conditions was also improved upon the inclusion of PPC. The lower charged defect density and the increased activation energy for ion migration were found to be responsible for the improved operational lifetime of the device based on PPC/perovskite composites.

Considering polymers with different functional groups, the incorporation of the optimal coordinating polymer P4VP[77] into the perovskite, through the developed interdiffusion method, was found to improve the operational stability of perovskite-based solar cells. The devices tested under ambient conditions (20–25 °C, RH 25–40%) under continuous AM 1.5-G 1 sun

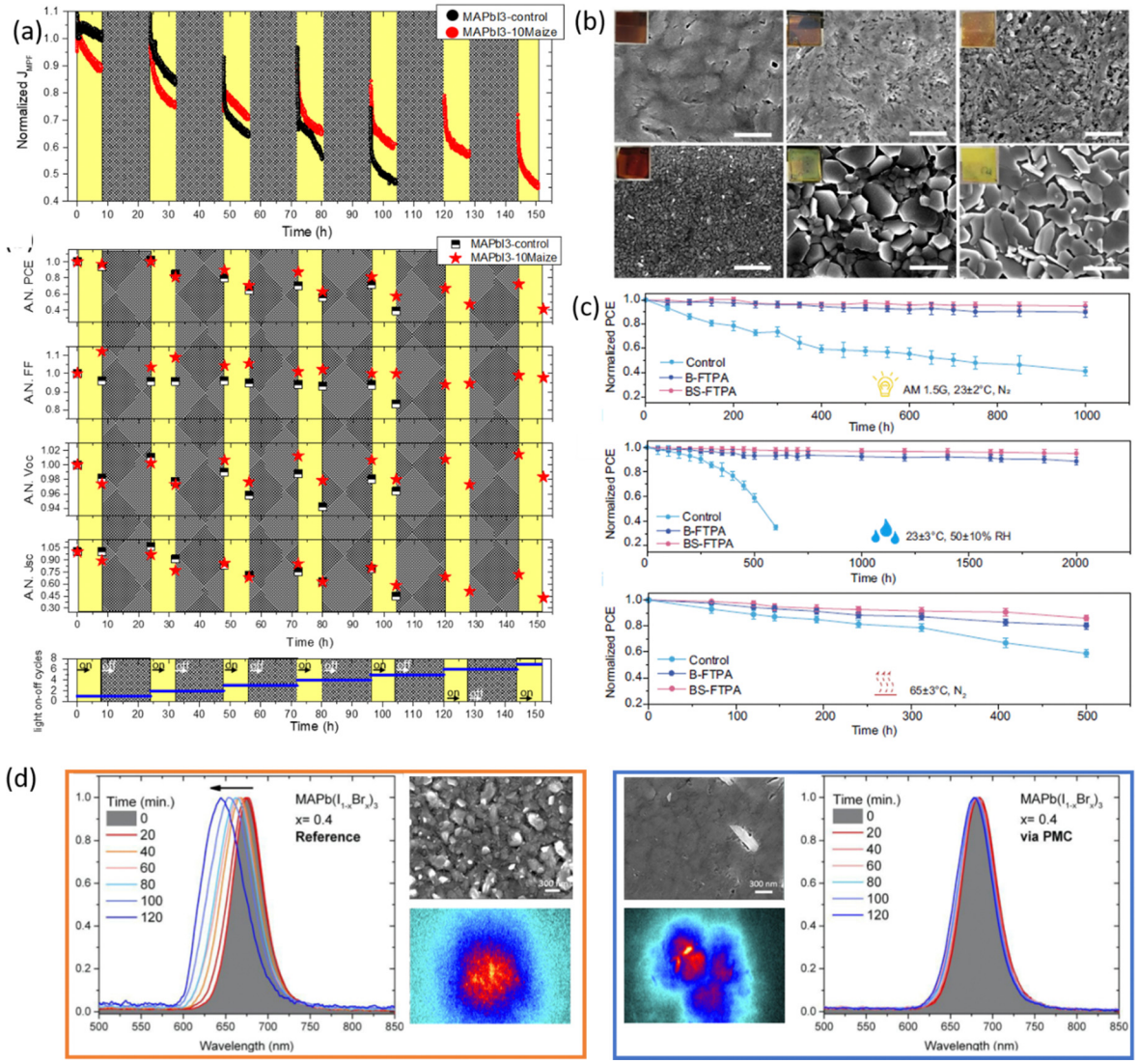


Fig. 8 Effect of polymer on perovskite stability. (a) The effect of maize on continuous MPP tracking for perovskite based solar cells measured under ISOS-LC-1-like aging conditions. Reproduced from ref. 31 with permission from the American Chemical Society, copyright 2022, under a Creative Commons Attribution 4.0 International License (CC BY 4.0); (b) SEM morphological analyses of perovskite films with and without HEC evidence and digital photo (inset) of thermal aging after 8 and 10 weeks under ISOS-T1I conditions, reproduced from ref. 32 with permission from Elsevier, copyright 2021; (c) device stability of unencapsulated devices under1-sun illumination at 23 ± 2 °C in a nitrogen atmosphere (ISOS-LC-1) (top), at 25 ± 5 °C and 50 ± 10% relative humidity (RH) (ISOS-D-1) (centre), under 65 ± 3 °C thermal aging (ISOS-T-1) (bottom), reproduced from ref. 36 with permission from Springer Nature, copyright 2023, under a Creative Commons Attribution 4.0 International License (CC BY 4.0); (d) laser induced photo-instability test on reference $MAPb(I_{0.6}Br_{0.4})_3$ without and gellan gum: PL spectra, SEM images and hyperspectral photoluminescence maps, reproduced from ref. 83 with permission from Royal Society of Chemistry, copyright 2023, under a Creative Commons Attribution 4.0 International License (CC BY 4.0).

illumination and constant bias voltage, showed a slight decrease in steady-state output power, after 30 min, in the presence of P4VP, despite the fast degradation of the pristine perovskite. In addition, the shelf time stability of the encapsulated devices stored in the glovebox was tested, observing a retention of more than 85% of the initial efficiency after more than three months in the presence of P4VP, with respect to the 59% of reduction shown by the bare perovskite. The authors speculated that the improved stability conferred by the introduction of the P4VP can be attributed to multiple effects related to the cross-linking of the grains induced by the polymer, or the reduction of water molecules access as well as ions migrations into the film.

Concerning lead-free perovskite, the influence on the operational stability of PVA/$FASnI_3$-based solar cells was investigated by measuring the photocurrent generated at the voltage close to the maximum power point $V_{MPP}$ under one-sun illumination and with encapsulation.[80] Compared to the bare perovskite, the device containing PVA showed stable efficiency after 400 h of continuous light irradiation. This is attributed to the strong hydrogen bonding interaction between the O–H group of PVA and $I^-$ in perovskite materials, which can hinder the migration

of unfavorable iodide ions, resulting in improved operational stability. Moreover, the antioxidant properties of the hydroxyl group contribute to enhancing the stability of the $FASnI_3$ film. Recently, great stability was observed by using FTPA-based polymer in the perovskite film, maintaining >95% of the initial efficiency for 1000 h under continuous sunlight soaking and for 2000 h at air ambient (~50% humidity) for the unencapsulated devices, thanks to the formation of the hydrogen-bonding polymer network in the perovskite film.[36] Li *et al.*[28] observed as well a high thermal stability with a retaining of 93.9% at 80 °C and 88.7% at −60 °C of the initial PCE value after 120 thermal cycles due to the strain-buffering effects induced by the inclusion of b-pV2F, demonstrating the resiliency of the crystal structure to temperature-induced strains.

Bisconti *et al.*[83] observed reduced photodegradation in the film deposited *via* GG-assisted crystallization without disturbing the photovoltaic performance. Indeed, the irreversible blue-shifted emission showed by the perovskite upon pulsed laser irradiation was not observed in the film containing GG, due to the formation of Br-rich domains following the disruption of the Pb–I bond, which is ascribed to photo-degradation, more stable due to a more compact morphology and to the mitigation of the decomposition of volatile MA cation and iodine species induced by the polysaccharides. Interestingly, the halide segregation process associated with the photoinduced reversible redshift was spatially confined in localized regions in the presence of GG, further confirming the superior endurance of the composite film to light exposure (Fig. 8(d)).

### 3.3. Polymer as a mechanical reinforcement of perovskite materials

Closely related to environmental stability, another major challenge currently limiting perovskite large-area manufacturing is the intrinsic mechanical fragility of the polycrystalline perovskite material. This inherent fragility makes the perovskite materials susceptible to the stresses generated during the fabrication procedure, which favours the formation of defects that, propagating into the film, would deteriorate the stability of the material itself. A key parameter used to quantify the thermo-mechanical reliability of the materials is represented by the fracture energy, Gc, which for perovskite films is $<1.5$ J m$^{-2}$ and is lower than any other photovoltaic technology. Therefore, improving the resistance to fracture is crucial to improve the operational durability and manufacturability of the material. A deep knowledge of the influence of the polymer on the perovskite crystallization process, thus on the final morphology of the film, is fundamental to understand how the distribution of the polymer within the film, relative to the perovskite grains, and a possible interaction with perovskite affect the mechanical behavior of the film. Of course, when the amount of polymer is high, and it is not used as an additive in small quantities, the final film can be considered a composite whose overall mechanical properties are strongly influenced by those of the polymer used.

Several methods were explored to enhance the mechanical properties of perovskite by including molecular additives, such as 5-aminovaleric acid (5-AVA),[96] or polymers with different functional groups, sometimes at the expense of solar cell efficiency. A recent result demonstrated that with the appropriate polymer it is possible to improve the thermomechanical properties of perovskite without compromising device performance.[31] For this purpose, the long chains of the starch polymer additive were used as a rheological modifier and templating agent, and to also confer also plasticity to the perovskite film, enhancing the resistance to bending stress and Gc of the material above 5 J m$^{-2}$. The developed nanocomposite is characterized by a uniform distribution of starch around the grain boundaries and throughout the film thickness, creating an intrinsic reinforcement for perovskite that improves the mechanical robustness and overall stability of the material, without hindering the high photoconversion efficiency of the device (Fig. 9(a)).

The effect of the addition of PU elastomer on the mechanical properties of $MAPbI_3$ perovskite was also studied by focusing on bending resistance. From EDS analysis, the amorphous PU was found to be distributed at the perovskite grain boundaries, acting as a cross-linker between the neighbouring perovskite crystals and limiting the breakage upon bending.[78] SEM images, acquired before and after mechanical bending applied 200 times with a bending radius of 1 cm, showed the formation of some cracks in the perovskite grain boundaries, differently from PU-perovskite films (Fig. 9(b)). The AFM peak-force model revealed a lower value of Young's modulus of PU-Perovskite film compared to the pristine perovskite, resulting in improved bendability due to the formation of a dense and highly elastic PU scaffold that cross-links the perovskite grain boundaries.

A composite matrix of SBS-PU was developed to improve the mechanical durability of perovskite for wearable PSCs.[72] The twisting of the device was investigated by studying its stability to bending and stretching, being the combination of the two. In both cases, an excellent tolerance was found for SBS-PU-based device, different from pristine perovskite, maintaining 80% of the initial PCE value after 5000 bending cycles, at a curvature radius of 2 mm, retaining 86% and 73% of the original PCE after 10% and 20% stretching tests, respectively, for 5000 cycles. In addition, the improvement in mechanical stability was investigated by measuring Young's modulus *via* deflection curves, observing a reduction (from 260 to 193 MPa) for SBS-PU-based perovskite that confirmed the improved toughness of the composite (Fig. 9(c)).

### 3.4. Influence of polymer on perovskite solution processability

The rise of high-efficiency perovskite devices has come at the expense of large-area manufacturing, as MHPs are still limited by deposition processing that overwhelmingly requires the use of antisolvent dripping or bath resulting in not straightforwardly up-scalable. Therefore, several research groups are focusing on the development of alternative deposition methods that can by-pass the antisolvent step, although still resulting in homogenous and pinhole-free perovskite film morphologies, which would be transferable to large-scale manufacturing of perovskite solar cells. Recently, different polysaccharides, such

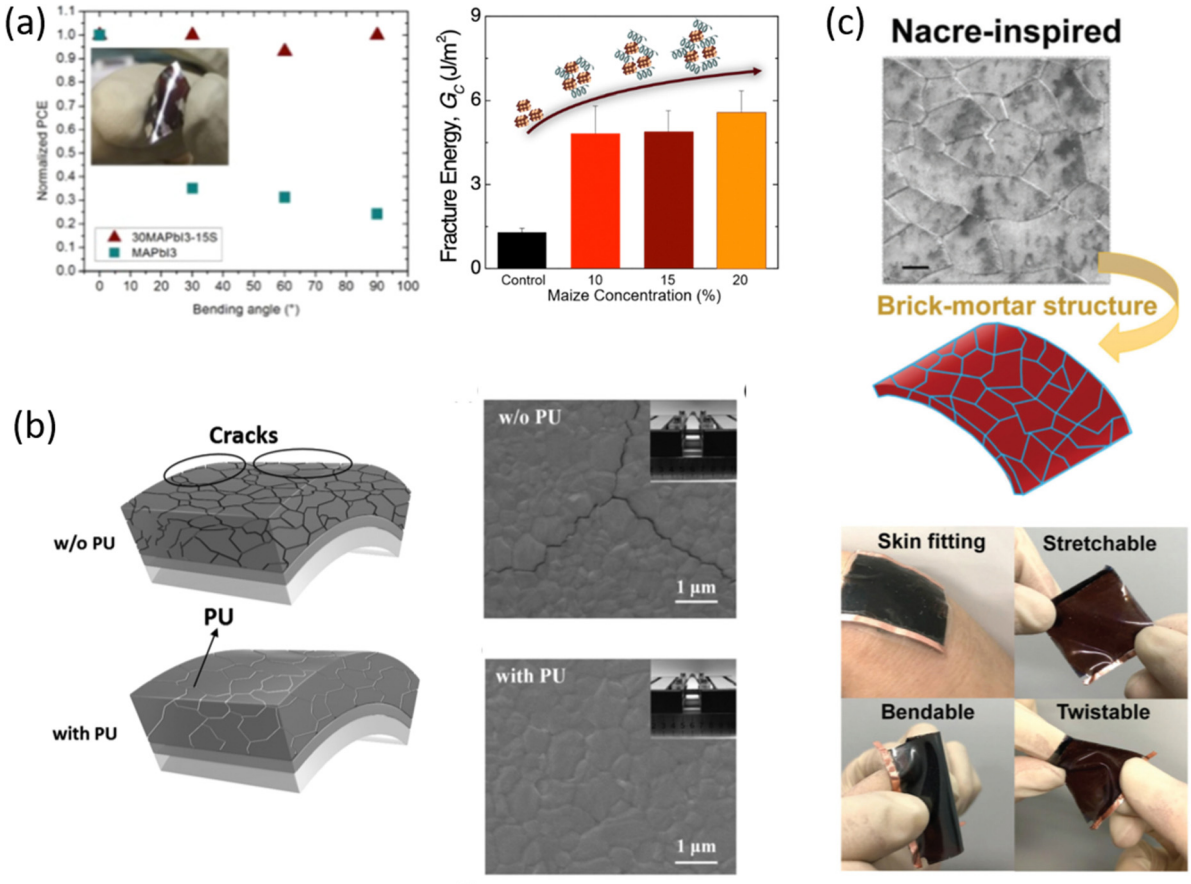


Fig. 9 Effect of the polymer on the mechanical properties of the perovskite material. (a) The effect of maize on the fracture energy of perovskite along with solar cell performance tolerance to bending stress, reproduced from ref. 27 with permission from Elsevier, copyright 2018, reproduced from ref. 31 with permission from the American Chemical Society, copyright 2022, under a Creative Commons Attribution 4.0 International License (CC BY 4.0); (b) a sketch of the effect of PU addition in perovskite films, along with SEM morphological evidence, reproduced from ref. 78 with permission from Wiley, copyright 2017; (c) photographs of the stretchable and wearable device based on SBS-PU. The compact perovskite morphology obtained *via* this approach is also reported, reproduced from ref. 72 with permission from the Royal Society of Chemistry.

as maize[24,25,27,41,74] and HEC[32] (at a high polymer/precursors ratio in DMSO solvent), have been used to delay and control the perovskite crystallization process in a single-step, antisolvent dripping free, deposition method (Fig. 10). Together with the strong influence on the perovskite growth process, the convenient viscosity modulation conferred by the polysaccharide to the perovskite precursor solution represents the key point to adapt the polymer/perovskite ink-formulation to the selected deposition technique. This allowed for the translation of the developed approach from lab-scale spin coating deposition[27] to different up-scalable techniques: inkjet printing,[74] slot die[25] coating up to roll to roll gravure printing technology.[24] The viscosity of the inks based on maize-perovskite was modified by simply varying the polymer-precursors concentration, making the formulation suitable to be used as ink-jet printable inks.[74] After the optimization of printing parameters (waveform, voltage, and temperature of the piezoelectrically driven print heads, drop space, substrate temperature), perovskite films were printed with uniform morphology, crystallinity, and tunable optical properties, demonstrating the versatility and scalability of the developed approach.

In 2021, a maize-perovskite composite was first deposited using the slot-die coating technique,[25] then using the roll-to-roll gravure printing,[24] confirming the possibility of printing the developed solution with high-throughput manufacturing technologies. The authors demonstrated the feasibility of obtaining a good morphology perovskite film at a mild temperature (60 °C) in an uncontrolled humid environment (RH up to 70%) in a single slot die printed step. The same composite was then deposited using the gravure printing method[24] without the use of an antisolvent-bath, thus significantly simplifying the process. The possibility to tune the rheology of the polymer–perovskite solution allowed an increase in viscosity of the inks up to values that were suitable for obtaining a high-resolution pattern using the gravure printing method. As a result, this reduced the perovskite precursor concentration by more than 50%, which is important in view of cost reduction. Optimization of deposition parameters resulted in printed films characterized by a fully converted perovskite phase and compact morphology that were implemented in flexible roll-to-roll processed solar cells with respectable PCEs.

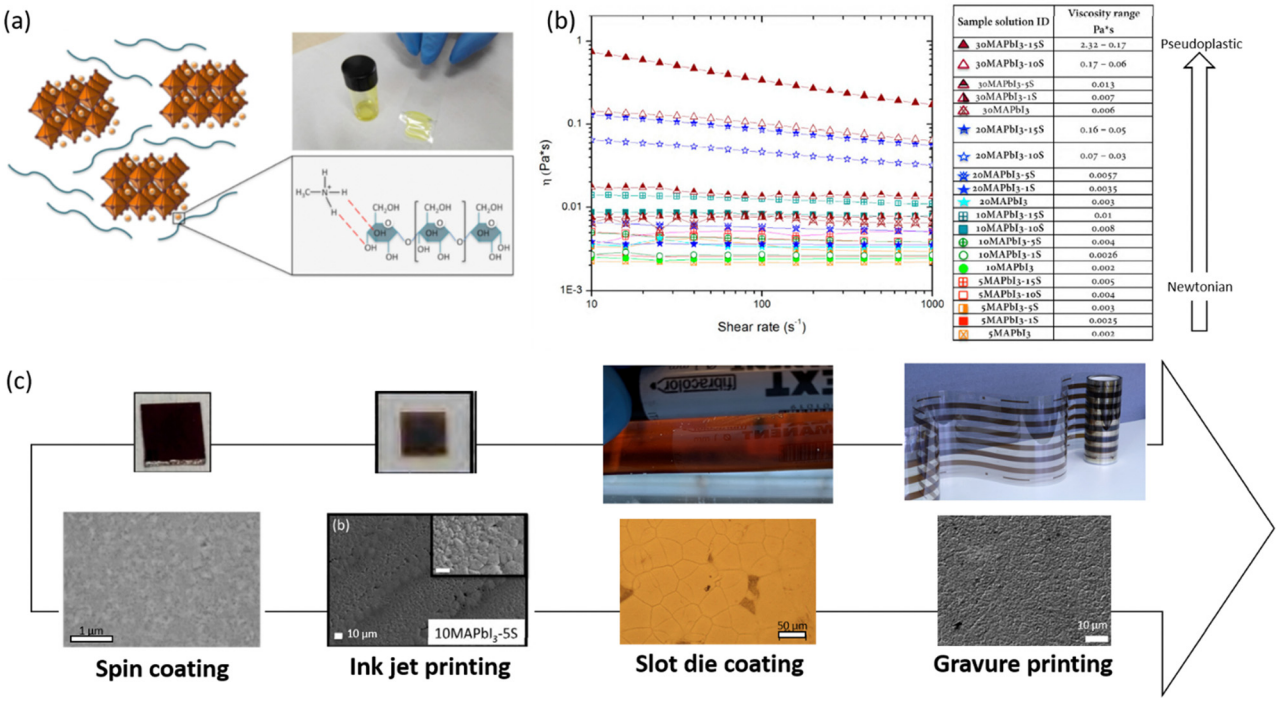


Fig. 10 The effect of maize polymer on solution processing on $MAPbI_3$ perovskite material. (a) A sketch representing the interaction of the starch polymer chain with perovskite material and a photograph of the starch/perovskite formulation with high viscosity; (b) steady viscosity as a function of shear rate by increasing perovskite precursor concentration and relative starch content, along with a table evidencing the viscosity modulation from Newtonian to pseudoplastic of starch/perovskite inks; (c) from lab scale to roll to roll deposition: Pictures and morphologies of the perovskite films grown using starch as additive obtained *via* different deposition techniques; reproduced from ref. 27 with permission from Elsevier, copyright 2018, reproduced with permission from ref. 25,74,75 with permission from MDPI, copyright 2008, Wiley copyright 2021, and Cell Press, under a Creative Commons Attribution 4.0 International License (CC BY 4.0).

## 4. Techniques for investigating perovskite crystallization: from interactions in solution to film formation

The perovskite crystallization process involves the evolution of complex dynamic equilibria among perovskite precursors, starting from the solution and continuing during film formation. Various chemical species can be present in the starting precursor solutions, spanning from monocation/monohalide systems (such as $FAPbI_3$ or $MAPbI_3$) to significantly more complex solutions simultaneously containing three cations (MA, FA, Cs) and two halides (I, Br).

The addition of a polymer involves modifying the coordination chemistry of the original solution, through establishing weak ionic, base–acid, and van de Waal interactions between ions and polymer, inter-ionic and inter-molecular forces between the polymer chains based on physical and chemical properties of the polymer. This results in a different equilibrium in solution and an assembly process where the polymer acts as a template for crystal growth.

The use of appropriate techniques to study these complex systems, from the investigation of chemical interaction with polymers already present in the perovskite precursor solution, is fundamental to better understand the influence of specific macromolecule properties on the perovskite self-assembly and obtain a complete picture of this situation.[97] With the aim of providing guidelines for approaching the characterization of the perovskite–polymer system, in the following, a summary of the most effective diagnostic tools used to investigate polymer/perovskite inks and their evolution into films is provided; in Fig. 11, and they are grouped and discussed based on the type of information that can be extracted:

-Characterization of the polymer/perovskite interaction in precursor inks;

-Characterization of the evolution from polymer/perovskite solutions to final films.

These techniques give critical information about the dyad polymer–perovskites and their interactions both in solution and the solid state.

**Nuclear magnetic resonance (NMR) spectroscopy** is an extremely powerful tool to investigate polymer perovskite precursor systems since it is one of the few that allows for studying both the solution and the interactions occurring among the nuclei belonging to the different species. Most importantly, based on the parameter analyzed, it can provide information on both the chemical nature of the species and their aggregation behaviour. In the work by Masi *et al.*,[29] among the NMR parameters, the focus was on diffusion coefficients ($D$, $m^2\ s^{-1}$), longitudinal relaxation times $T1$ (s) and transverse relaxation times $T2$ (s), which are expected to be responsive to aggregation

phenomena. This work demonstrated the correlation of established interactions with the final film morphology. Indeed, a higher decrease in relaxation parameters determines films with more interconnected domains based on interactions between polymers and precursors that guide the self-assembly process of the perovskite crystals. They observed the formation of hydrogen bonds between $MA^+$ acid hydrogen atoms and electron-rich atoms belonging to the polymer through ether functional groups of MEH-PPV and nitrogen atoms of the pending moieties of PFN. Instead, a significant reduction of interactions with MA was observed for the polymers characterized by a reduced availability of electron pairs, such as PMMA and PTAA or without hydrogen bonds of donor/acceptor groups like in polystyrene, resulting in inhomogeneous films and poor substrate coverage.[30] This was one of the first studies providing a fundamental tool to study the chemical–physical interactions taking place in solution between perovskite precursors and polymers, predicting the properties of the final film.

Fourier transform infrared (FTIR) spectroscopy is also a key and widely employed tool for identifying some intermediate states. For PMMA/perovskite composites,[33] FTIR measurements evidenced the formation of an intermediate adduct between the carbonyl groups of the polymer and $PbI_2$ by shifting the characteristic stretching vibration of the C═O bond from 1735 $cm^{-1}$ for pure PMMA to 1723 $cm^{-1}$ upon $PbI_2$ inclusion. The weakening of the C═O bond strength induced by the interaction with the Lewis acid $PbI_2$ causes a shift towards lower wavenumbers. This adduct slows down the self-assembly process and results in a high-quality perovskite film. In another work, a polymer–perovskite composite cross-linker, *i.e.*, $CH_3NH_3I{\cdot}PbI_2{\cdot}DMF{\cdot}DMSO$.– Polymeric Lewis base (poly(propylene carbonate, PPC)[35] was used with the aim of forming macro-molecular intermediate phases. FTIR spectroscopy was used to study the influence of the molecular dipole and structure of PPC on the interaction with perovskite precursors to evaluate the effect of intermediate phase formation on perovskite crystallization. Without the polymeric Lewis base, the N–H stretch ($\nu1$(asym) = 3161 $cm^{-1}$, $\nu2$(sym) = 3124 $cm^{-1}$) of the adduct powder shifted upon DMSO addition, indicating the interaction $NH_3^+$ of the MAI with the solvent that is a Lewis base itself. Upon inclusion of PPC polymer, which has a higher dipole moment than DMSO, a more pronounced shift to ($\nu1$(asym) = 3199 $cm^{-1}$, $\nu2$(sym) = 3162 $cm^{-1}$) was recorded. The C═O stretching of the polymer in the presence of the

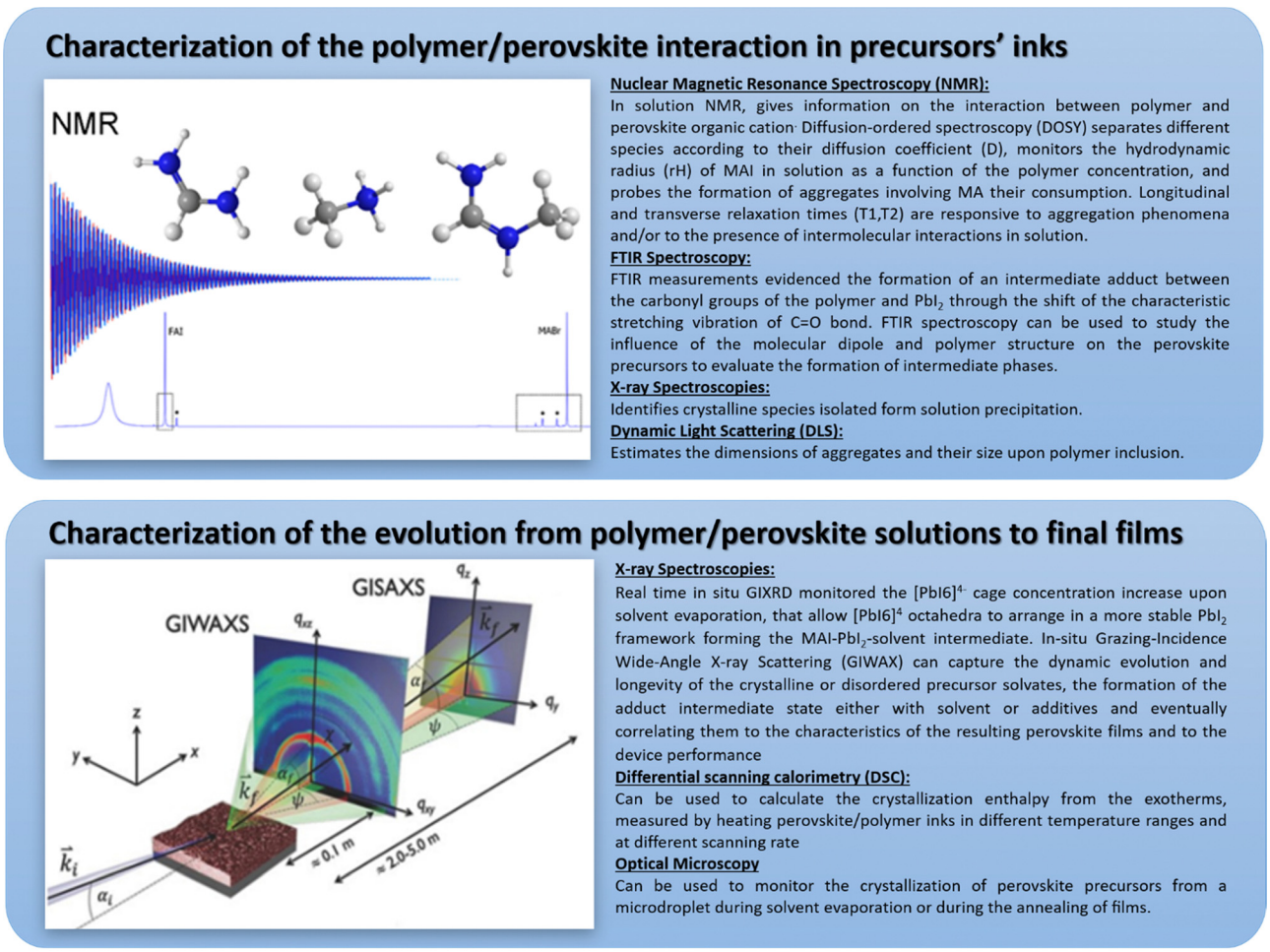


Fig. 11 A summary of the most used characterization tools for the investigation of polymer/metal-halide perovskite composites from the interaction in solution to film formation, reproduced from ref. 97 with permission from Elsevier.

Lewis-base adduct $CH_3NH_3I{\cdot}PbI_2{\cdot}DMSO{\cdot}$ also redshifted from 1760 $cm^{-1}$ to 1743 $cm^{-1}$ for pure PPC. The characteristic C=O stretch peaks around 1789 $cm^{-1}$ observed in the actual perovskite films suggest the presence of the Lewis bases.

X-ray diffraction (XRD) has also been used to study intermediate species, thus to reveal polymer:perovskite interactions to evaluate how the formation of adducts influences perovskite crystal growth. Han *et al.*[35] observed that most of the peaks below 10° of the synthesized adduct powders with DMSO or PPC disappeared after crystallization due to the interplanar distances of the adducts longer than that of the pure perovskite disappeared. Thus, the XRD peaks of the adduct powder provide information on the molecular ordering of the intermediate phases.

XRD can also provide important information about the crystalline phase evolution of perovskite materials with annealing. Zhao *et al.*[34] monitor the crystallization of $MAPbI_3$ perovskite in polyethylene glycol (PEG) scaffolds using XRD to track the evolution of the intermediate phase peaks in the 10°–20° range over the course of annealing with respect to the characteristic (110) and (220) peaks of perovskite phase. In the case of pristine perovskite, the intermediate phase disappeared and the complete conversion to crystalline perovskite materials occurred, visible as strong (110) and (220) peaks, upon 70 min of annealing at 105 °C. Instead, in the presence of PEG, the intermediate phase is more long-lived and the intermediate phase disappeared after 90 min, evidencing the influence of the polymer macromolecule in slowing down the crystallization process of perovskite.

Very simple and readily available methods can contribute to determining the kinetics of nucleation and crystallization, such as differential scanning calorimetry (DSC) that has been shown to be very effective in shedding light on the kinetic and thermodynamic evolution of the perovskite crystallization process.[41] Perovskite inks can be heated in different temperature ranges and at different scanning rates and the crystallization enthalpy, temperature and time can be calculated from the exotherms.

Similar information can be extracted by Thermogravimetric analysis (TGA). TGA revealed substantially increased sublimation temperature on polypropylene carbonate-perovskite precursor adducts[35] due to the formation of the polymeric adduct. This effect was attributed to the donation of the lone pair electrons on the oxygen of the Lewis bases to $CH_3NH_3^+$ and $PbI_2$ that results in the formation of a $CH_3NH_3I{\cdot}PbI_2{\cdot}DMSO{\cdot}$Lewis-base adduct, and the addition of a Lewis base with a higher permanent dipole can more chemically stabilize the adduct formation.

The most informative techniques for monitoring the evolution from polymer/perovskite precursor solution to film are in-situ and time-resolved X-ray scattering techniques. A powerful custom-made technique, the time-resolved in-situ Grazing-Incidence Wide-Angle X-ray Scattering (GIWAXS), provides information on the real deposition process through the use of synchrotron radiation during the spin-coating process,[41] correlating it to the perovskite crystallization. In detail, the characteristic fingerprints of crystalline or disordered precursor solvates, the presence and longevity of the intermediate adduct phase, and the resulting perovskite phase were monitored as a function of different parameters (*i.e.* solvents, additives, spin-coating rate *etc.*). Giuri *et al.* observed that the inclusion of starch polymer in the $MAPbI_3$ precursor solution forms a sol–gel network within the precursor solutions that is responsible for delaying the self-assembly process of perovskite.[41] Instead, Li *et al.*[28] observed faster perovskite conversion in the presence of β-pV2F. They monitored several different stages that characterized the film formation from the initial stage ($t_1$) characterized by the scattering halo due to the presence of the solvated colloidal sol precursor, to the dripping stage ($t_2$) with the disappearance of the diffraction signal due to the rapid solvent extraction, the next spin coating stage ($t_3$) characterized by the appearance of the supersaturated solvate intermediate followed by its evolution during the annealing process due to the perovskite crystal growth.

Rheology is another additional characterization that allows us to link the characteristics of the solutions to the ones of the films through monitoring nucleation. It has been demonstrated,[27] for example, that the viscosity tuning of a MAPI:starch composite is a very powerful tool to control the morphology of the film, the thickness and the grain size, thanks to the widening of the time frame within which the crystallization of perovskite occurs.[41]

Energy dispersive spectroscopy (EDS) analysis in a Cs-corrected scanning transmission electron microscope (STEM) was performed by Zhao *et al.*[34] on the PEG-perovskite composite, confirming that PEG acted as a scaffold in the perovskite film. The high-angle annular dark field (HAADF) STEM image along with the EDS mapping of O element, which is only contained in PEG, revealed that the amorphous polymeric material is located at the perovskite grains, surrounding them.

The combination of scanning electron microscope (SEM) and EDS characterizations represents a useful tool to detect the presence of polymer in the crystallized film. Giuri *et al.*[31] evidenced the homogeneous distribution of Maize in the perovskite film throughout the thickness of the polymer/perovskite composite films.

Transmission electron microscopy (TEM) was used by Han *et al.*[35] to evidence the inter-grain cross-linker role of PPC, which determines the formation of a 'bridge' between two perovskite grains, affecting the crystal growth and the electrical properties of the film, due to the reduction of grain-to-grain electrical decoupling.

## 5. Conclusions and outlook

The emergence of MHP as the active layer of solar cells has revolutionized the field of photovoltaics due to the extraordinary optoelectronic properties of the material. However, even if in the last years the performances of PSCs have tremendously improved, their commercialization is still hindered by several aspects, mostly related to the processability and stability issues of MHPs. The transition from laboratory-scale to large-scale requires the development of MHP-based inks compatible with printing technologies allowing the deposition, in a reproducible fashion, of large area high-quality films. Therefore, fine control of the perovskite film formation process is a necessary condition.

Envisioning MHP devices up-scaling, the use of polymer as a templating agent has proven to be an effective strategy to improve the material crystallization process, towards simple solution processability, along with its environmental and thermo-mechanical stability.

This review focused on the main features related to the use of polymers for the development of MHP-based inks. From the first developed polymer/MHP composite film (2015) to now, several aspects related to the use of this approach have been better understood: (i) polymeric additives play an important role during the MHP crystallization process by controlling nucleation and precursor assembly processes, with a direct influence on the crystallite size and morphology of the films. The appropriate selection of the functional groups of the polymer can lead to specific interaction with perovskite precursors resulting in enhanced efficiency and reduced degradation rates. (ii) Polymer usually locate at the grain boundaries of the perovskite material, acting therefore as a passivating/protecting agent, making the resulting films mechanically more robust to fracture processes, as witnessed by the increase of the maize:perovskite film Gc above 5 J $m^{-2}$. (iii) From a manufacturing viewpoint, the use of polymers (especially polysaccharides) can considerably simplify the processability of MHPs, enabling their deposition without the use of toxic antisolvent treatments, achieving performances of around 19%. Meanwhile, withstanding antisolvent-assisted deposition, high power conversion efficiencies, above 24%, were achieved with the use of polymers as a controlling agent of the perovskite film formation.

However, besides the great advantages gained from using the polymer to assist the perovskite crystallization, the insulating nature of itself represents an issue to be considered. Hence proper engineering of the perovskite inks, especially concerning the ratio between polymer/perovskite, is the starting point towards high-quality and performance films. This approach allows not only for multiple implications on the properties of the final film, but also for engineering the material according to the type of manufacturing process used and/or the type of final application. The outlook for this approach is very promising. Indeed, especially if the polymer allows control of the crystallization process without the use of any dripping, as in most of our studies, polymer perovskite alloying can offer superior MHP processability and devices with longer operational lifetimes, withstanding industrially diffused printing techniques, fostering thus the commercialization of this technology.

## Conflicts of interest

There are no conflicts to declare.

## Acknowledgements

The authors gratefully acknowledge the PNRR MUR project: ''Integrated Infrastructure Initiative in Photonic and Quantum Sciences'' – I-PHOQS (IR0000016); the authors gratefully acknowledge the project ''Mission Innovation, IEMAP'' founded by the Ministero della Transizione Ecologica, MiTE (CUP B82C2100-1820001). The authors gratefully acknowledge the project ''New concepts, materials and technologies for the building integration of photovoltaics in a scenario of diffuse generation'' (CANVAS) founded by the Italian Ministry of the Environment and the Energy Security, through the Research Fund for the Italian Electrical System (type-A call, published on G.U.R.I. n. 192 on 18-08-2022). AR acknowledges the project Ricerca@Cnr VertiGrow (CUP B15F21004410005). SC acknowledges the project Ricerca@Cnr PHOTOCAT (CUP B93C21000060006).

## References

1 N. R. E. L. (NREL), Best Research-Cell Efficiencies Chart, 2023.
2 Z. Dai, S. K. Yadavalli, M. Chen, A. Abbaspourtamijani, Y. Qi and N. P. Padture, *Science*, 2021, **372**, 618.
3 W. Hui, L. Chao, H. Lu, F. Xia, Q. Wei, Z. Su, T. Niu, L. Tao, B. Du and D. Li, *Science*, 2021, **371**, 1359.
4 H. Min, D. Y. Lee, J. Kim, G. Kim, K. S. Lee, J. Kim, M. J. Paik, Y. K. Kim, K. S. Kim and M. G. Kim, *Nature*, 2021, **598**, 444.
5 D. Liu and T. L. Kelly, *Nat. Photonics*, 2014, **8**, 133.
6 N. J. Jeon, J. H. Noh, Y. C. Kim, W. S. Yang, S. Ryu and S. Il Seok, *Nat. Mater.*, 2014, **13**, 897.
7 H. Wei, Y. Fang, P. Mulligan, W. Chuirazzi, H.-H. Fang, C. Wang, B. R. Ecker, Y. Gao, M. A. Loi and L. Cao, *Nat. Photonics*, 2016, **10**, 333.
8 Q. Jiang, L. Zhang, H. Wang, X. Yang, J. Meng, H. Liu, Z. Yin, J. Wu, X. Zhang and J. You, *Nat. Energy*, 2016, **2**, 1.
9 M. Shi, H. Zhou, W. Tian, B. Yang, S. Yang, K. Han, R. Li and C. Li, *Cell Rep. Phys. Sci.*, 2021, 100656.
10 M. A. Green, A. Ho-Baillie and H. J. Snaith, *Nat. Photonics*, 2014, **8**, 506.
11 A. S. R. Bati, Y. L. Zhong, P. L. Burn, M. K. Nazeeruddin, P. E. Shaw and M. Batmunkh, *Commun. Mater.*, 2023, **4**, 2.
12 S. D. Stranks and H. J. Snaith, *Nat. Nanotechnol.*, 2015, **10**, 391.
13 S. Colella, M. Mazzeo, A. Rizzo, G. Gigli and A. Listorti, *J. Phys. Chem. Lett.*, 2016, **7**, 4322.
14 J. Miao and F. Zhang, *J. Mater. Chem. C*, 2019, **7**, 1741.
15 H. Wei and J. Huang, *Nat. Commun.*, 2019, **10**, 1.
16 H. Wu, Y. Ge, G. Niu and J. Tang, *Matter*, 2021, **4**, 144.
17 C. Liang, P. Li, H. Gu, Y. Zhang, F. Li, Y. Song, G. Shao, N. Mathews and G. Xing, *Sol. RRL*, 2018, **2**, 1700217.
18 F. Schackmar, H. Eggers, M. Frericks, B. S. Richards, U. Lemmer, G. Hernandez-Sosa and U. W. Paetzold, *Adv. Mater. Technol.*, 2021, **6**, 2000271.
19 J. E. Bishop, J. A. Smith and D. G. Lidzey, *ACS Appl. Mater. Interfaces*, 2020, **12**, 48237.
20 L.-H. Chou, J. M. W. Chan and C.-L. Liu, *Sol. RRL*, 2022, **6**, 2101035.
21 C. Chen, J. Chen, H. Han, L. Chao, J. Hu, T. Niu, H. Dong, S. Yang, Y. Xia and Y. Chen, *Nature*, 2022, 1.
22 Y. Y. Kim, T.-Y. Yang, R. Suhonen, A. Kemppainen, K. Hwang, N. J. Jeon and J. Seo, *Nat. Commun.*, 2020, **11**, 1.

23 K. Hwang, Y. Jung, Y. Heo, F. H. Scholes, S. E. Watkins, J. Subbiah, D. J. Jones, D. Kim and D. Vak, *Adv. Mater.*, 2015, **27**, 1241.
24 F. Bisconti, A. Giuri, R. Suhonen, T. M. Kraft, M. Ylikunnari, V. Holappa, P. Biagini, A. Savoini, G. Marra and S. Colella, *Cell Rep. Phys. Sci.*, 2021, **2**, 100639.
25 F. Bisconti, A. Giuri, G. Marra, A. Savoini, P. Fumo, R. Marrazzo, S. Zanardi, G. Corso, R. Po and P. Biagini, *ChemPlusChem*, 2021, **86**, 1442.
26 K. Kim, J. Han, S. Maruyama, M. Balaban and I. Jeon, *Sol. RRL*, 2021, **5**, 2000783.
27 A. Giuri, S. Masi, A. Listorti, G. Gigli, S. Colella, C. E. Corcione and A. Rizzo, *Nano Energy*, 2018, **54**, 400.
28 G. Li, Z. Su, L. Canil, D. Hughes, M. H. Aldamasy, J. Dagar, S. Trofimov, L. Wang, W. Zuo and J. J. Jerónimo-Rendon, *Science*, 2023, **379**, 399.
29 S. Masi, A. Rizzo, F. Aiello, F. Balzano, G. Uccello-Barretta, A. Listorti, G. Gigli and S. Colella, *Nanoscale*, 2015, **7**, 18956.
30 S. Masi, S. Colella, A. Listorti, V. Roiati, A. Liscio, V. Palermo, A. Rizzo and G. Gigli, *Sci. Rep.*, 2015, **5**, 7725.
31 A. Giuri, N. Rolston, S. Colella, A. Listorti, C. Esposito Corcione, H. Elmaraghi, S. Lauciello, R. H. Dauskardt and A. Rizzo, *ACS Appl. Energy Mater.*, 2021, **4**, 11194–11203.
32 F. Bisconti, A. Giuri, L. Dominici, S. Carallo, E. Quadrivi, P. Biagini, A. Listorti, C. E. Corcione, S. Colella and A. Rizzo, *Nano Energy*, 2021, **89**, 106406.
33 D. Bi, C. Yi, J. Luo, J.-D. Décoppet, F. Zhang, S. M. Zakeeruddin, X. Li, A. Hagfeldt and M. Grätzel, *Nat. Energy*, 2016, **1**, 16142.
34 Y. Zhao, J. Wei, H. Li, Y. Yan, W. Zhou, D. Yu and Q. Zhao, *Nat. Commun.*, 2016, **7**, 10228.
35 T.-H. Han, J.-W. Lee, C. Choi, S. Tan, C. Lee, Y. Zhao, Z. Dai, N. De Marco, S.-J. Lee, S.-H. Bae, Y. Yuan, H. M. Lee, Y. Huang and Y. Yang, *Nat. Commun.*, 2019, **10**, 520.
36 M. Li, R. Sun, J. Chang, J. Dong, Q. Tian, H. Wang, Z. Li, P. Yang, H. Shi and C. Yang, *Nat. Commun.*, 2023, **14**, 573.
37 J. C. Hamill Jr, J. Schwartz and Y.-L. Loo, *ACS Energy Lett.*, 2017, **3**, 92.
38 J. Wang, W. Li and W.-J. Yin, *Adv. Mater.*, 2020, **32**, 1906115.
39 B. Li, Q. Zhang, S. Zhang, Z. Ahmad, T. Chidanguro, A. Hunter Davis, Y. C. Simon, X. Gu, W. Zheng, N. Pradhan and Q. Dai, *Chem. Eng. J.*, 2021, **405**, 126998.
40 K. Yan, M. Long, T. Zhang, Z. Wei, H. Chen, S. Yang and J. Xu, *J. Am. Chem. Soc.*, 2015, **137**, 4460.
41 A. Giuri, R. Munir, A. Listorti, C. E. Corcione, G. Gigli, A. Rizzo, A. Amassian and S. Colella, *Nanotechnology*, 2021, **32**, 265707.
42 H. J. Snaith, *Nat. Mater.*, 2018, **17**, 372.
43 C. J. Bartel, C. Sutton, B. R. Goldsmith, R. Ouyang, C. B. Musgrave, L. M. Ghiringhelli and M. Scheffler, *Sci. Adv.*, 2019, **5**, eaav0693.
44 V. M. Goldschmidt, *Naturwissenschaften*, 1926, **14**, 477.
45 D. B. Mitzi, S. Wang, C. A. Feild, C. A. Chess and A. M. Guloy, *Science*, 1995, **267**, 1473.
46 N.-G. Park, *Mater. Today*, 2015, **18**, 65.
47 P. Tonui, S. O. Oseni, G. Sharma, Q. Yan and G. T. Mola, *Renew. Sustain. Energy Rev.*, 2018, **91**, 1025.
48 J.-P. Correa-Baena, A. Abate, M. Saliba, W. Tress, T. J. Jacobsson, M. Grätzel and A. Hagfeldt, *Energy Environ. Sci.*, 2017, **10**, 710.
49 M. Saliba, J. Correa-Baena, M. Grätzel, A. Hagfeldt and A. Abate, *Angew. Chem., Int. Ed.*, 2018, **57**, 2554.
50 K. H. Girish, K. A. Vishnumurthy and T. S. Roopa, *Mater. Today Sustainable*, 2022, **17**, 100090.
51 R. Mastria, S. Colella, A. Qualtieri, A. Listorti, G. Gigli and A. Rizzo, *Nanoscale*, 2017, **9**, 3889.
52 H. Hu, M. Singh, X. Wan, J. Tang, C.-W. Chu and G. Li, *J. Mater. Chem. A*, 2020, **8**, 1578.
53 C. Liu, Y.-B. Cheng and Z. Ge, *Chem. Soc. Rev.*, 2020, **49**, 1653.
54 N. T. K. Thanh, N. Maclean and S. Mahiddine, *Chem. Rev.*, 2014, **114**, 7610.
55 W. Ostwald, *Z. Physiol. Chem.*, 1900, **34U**, 495.
56 Y. Guo, K. Shoyama, W. Sato, Y. Matsuo, K. Inoue, K. Harano, C. Liu, H. Tanaka and E. Nakamura, *J. Am. Chem. Soc.*, 2015, **137**, 15907.
57 N. D. Pham, V. T. Tiong, D. Yao, W. Martens, A. Guerrero, J. Bisquert and H. Wang, *Nano Energy*, 2017, **41**, 476.
58 L. Zhi, Y. Li, X. Cao, Y. Li, X. Cui, D. Zhuang, L. Ci, J. Wei and A. C. S. Appl, *Energy Mater.*, 2019, **2**, 320.
59 Y. Zhou, M. Yang, W. Wu, A. L. Vasiliev, K. Zhu and N. P. Padture, *J. Mater. Chem. A*, 2015, **3**, 8178.
60 Z. Xiao, Q. Dong, C. Bi, Y. Shao, Y. Yuan and J. Huang, *Adv. Mater.*, 2014, **26**, 6503.
61 X. Cao, L. Zhi, Y. Li, F. Fang, X. Cui, L. Ci, K. Ding, J. Wei and A. C. S. Appl, *Energy Mater.*, 2018, **1**, 868.
62 C. Liu, K. Wang, C. Yi, X. Shi, A. W. Smith, X. Gong and A. J. Heeger, *Adv. Funct. Mater.*, 2016, **26**, 101.
63 H. Hu, Z. Ren, P. W. K. Fong, M. Qin, D. Liu, D. Lei, X. Lu and G. Li, *Adv. Funct. Mater.*, 2019, **29**, 1900092.
64 L.-L. Gao, C.-X. Li, C.-J. Li and G.-J. Yang, *J. Mater. Chem. A*, 2017, **5**, 1548.
65 M. Zhang, H. Yu, J.-H. Yun, M. Lyu, Q. Wang and L. Wang, *Chem. Commun.*, 2015, **51**, 10038.
66 S. Sanchez, X. Hua, N. Phung, U. Steiner and A. Abate, *Adv. Energy Mater.*, 2018, **8**, 1702915.
67 E. Parvazian, A. Abdollah-zadeh, H. R. Akbari and N. Taghavinia, *Sol. Energy Mater. Sol. Cells*, 2019, **191**, 148.
68 K. G. Stamplecoskie, J. S. Manser and P. V. Kamat, *Energy Environ. Sci.*, 2015, **8**, 208.
69 S. Masi, A. Rizzo, R. Munir, A. Listorti, A. Giuri, C. Esposito Corcione, N. D. Treat, G. Gigli, A. Amassian, N. Stingelin and S. Colella, *Adv. Energy Mater.*, 2017, 7, DOI: **10.1002/aenm.201602600**.
70 C. Bi, Q. Wang, Y. Shao, Y. Yuan, Z. Xiao and J. Huang, *Nat. Commun.*, 2015, **6**, 7747.
71 Q. Wang, B. Chen, Y. Liu, Y. Deng, Y. Bai, Q. Dong and J. Huang, *Energy Environ. Sci.*, 2017, **10**, 516.
72 X. Hu, Z. Huang, F. Li, M. Su, Z. Huang, Z. Zhao, Z. Cai, X. Yang, X. Meng, P. Li, Y. Wang, M. Li, Y. Chen and Y. Song, *Energy Environ. Sci.*, 2019, **12**, 979.
73 J.-E. Kim, S.-S. Kim, C. Zuo, M. Gao, D. Vak and D.-Y. Kim, *Adv. Funct. Mater.*, 2019, **29**, 1809194.
74 A. Giuri, E. Saleh, A. Listorti, S. Colella, A. Rizzo, C. Tuck and C. Esposito Corcione, *Nanomaterial*, 2019, 9, DOI: **10.3390/nano9040582**.

75 F. *et al.* Bisconti, Cell Reports Phys. Sci. Accept. Publ. n.d.
76 C.-Y. Chang, C.-Y. Chu, Y.-C. Huang, C.-W. Huang, S.-Y. Chang, C.-A. Chen, C.-Y. Chao and W.-F. Su, *ACS Appl. Mater. Interfaces*, 2015, **7**, 4955.
77 L. Zuo, H. Guo, S. Jariwala, N. De Marco, S. Dong, R. DeBlock, D. S. Ginger, B. Dunn, M. Wang and Y. Yang, *Sci. Adv.*, 2017, **3**, e1700106.
78 Z. Huang, X. Hu, C. Liu, L. Tan and Y. Chen, *Adv. Funct. Mater.*, 2017, **27**, 1703061.
79 J. Hong, H. Kim and I. Hwang, *Org. Electron.*, 2019 **73**, 87.
80 X. Meng, J. Lin, X. Liu, X. He, Y. Wang, T. Noda, T. Wu, X. Yang and L. Han, *Adv. Mater.*, 2019, **31**, 1903721.
81 Y. Ren, Y. Hao, N. Zhang, Z. Arain, M. Mateen, Y. Sun, P. Shi, M. Cai and S. Dai, *Chem. Eng. J.*, 2020, **392**, 123805.
82 Q. Cao, Y. Li, H. Zhang, J. Yang, J. Han, T. Xu, S. Wang, Z. Wang, B. Gao and J. Zhao, *Sci. Adv.*, 2021, **7**, eabg0633.
83 F. Bisconti, M. Leoncini, G. Bravetti, A. Giuri, L. Polimeno, S. Carallo, S. Colella, L. Gatto, F. Grandi, E. Cinquanta, C. Vozzi, S. Gambino, L. Dominici and A. Rizzo, *J. Mater. Chem. C*, 2023, DOI: **10.1039/D3TC01833D**.
84 M. Leoncini, R. Giannuzzi, A. Giuri, S. Colella, A. Listorti, V. Maiorano, A. Rizzo, G. Gigli and S. Gambino, *J. Sci. Adv. Mater. Dev.*, 2021, **6**, 543.
85 A. Giuri, Z. Yuan, Y. Miao, J. Wang, F. Gao, N. Sestu, M. Saba, G. Bongiovanni, S. Colella and C. E. Corcione, *Sci. Rep.*, 2018, **8**, 15496.
86 M. Verdi, A. Giuri, A. Ciavatti, A. Rizzo, C. Esposito Corcione, L. Basiricò, S. Colella and B. Fraboni, *Adv. Mater. Interfaces*, 2023, 2300044.
87 J. H. E. Cartwright, J. M. Garcıa-Ruiz and A. I. Villacampa, *Comput. Phys. Commun.*, 1999, **121**, 411.
88 M. V. Khenkin, E. A. Katz, A. Abate, G. Bardizza, J. J. Berry, C. Brabec, F. Brunetti, V. Bulović, Q. Burlingame and A. Di Carlo, *Nat. Energy*, 2020, **5**, 35.
89 S. Tan, T. Huang, I. Yavuz, R. Wang, M. H. Weber, Y. Zhao, M. Abdelsamie, M. E. Liao, H.-C. Wang and K. Huynh, *J. Am. Chem. Soc.*, 2021, **143**, 6781.
90 S. Tan, I. Yavuz, M. H. Weber, T. Huang, C.-H. Chen, R. Wang, H.-C. Wang, J. H. Ko, S. Nuryyeva and J. Xue, *Joule*, 2020, **4**, 2426.
91 Z. Zhu, K. Mao, K. Zhang, W. Peng, J. Zhang, H. Meng, S. Cheng, T. Li, H. Lin and Q. Chen, *Joule*, 2022, **6**, 2849.
92 B. L. Watson, N. Rolston, A. D. Printz and R. H. Dauskardt, *Energy Environ. Sci.*, 2017, **10**, 2500.
93 N. Rolston, B. L. Watson, C. D. Bailie, M. D. McGehee, J. P. Bastos, R. Gehlhaar, J.-E. Kim, D. Vak, A. T. Mallajosyula and G. Gupta, *Extrem. Mech. Lett.*, 2016, **9**, 353.
94 G. Grancini and M. K. Nazeeruddin, *Nat. Rev. Mater.*, 2019, **4**, 4.
95 A. K. Jena, A. Kulkarni and T. Miyasaka, *Chem. Rev.*, 2019, **119**, 3036.
96 M. Gutwald, N. Rolston, A. D. Printz, O. Zhao, H. Elmaraghi, Y. Ding, J. Zhang and R. H. Dauskardt, *Sol. Energy Mater. Sol. Cells*, 2020, **209**, 110433.
97 A. Rizzo, A. Listorti and S. Colella, *Chem*, 2022, **8**, 31.